The Mechanism of Lamellar-to-Inverted Hexagonal Phase Transitions in Phosphatidylethanolamine: Implications for Membrane Fusion Mechanisms

D. P. Siegel* and R. M. Epand#
*Procter & Gamble Company, Cincinnati, Ohio 45253 USA, and #Department of Biochemistry, McMaster University, Hamilton, Ontario L8N 3Z5, Canada

ABSTRACT We studied the mechanism of the lamellar-to-inverted hexagonal (L_α/H_{II}) phase transition, using time-resolved cryotransmission electron microscopy (TRC-TEM), ^{31}P-NMR, and differential scanning calorimetry. The transition was initiated in dispersions of large unilamellar vesicles of dipalmitoleoyl phosphatidylethanolamine (DiPoPE). We present evidence that the transition proceeds in three steps. First, many small connections form between apposed membranes. Second, the connections aggregate within the planes of the bilayers, forming arrays with hexagonal order in some projections. Third, these quasihexagonal structures elongate into small domains of H_{II} phase, acquiring lipid molecules by diffusion from contiguous bilayers. A previously proposed membrane fusion mechanism rationalizes these results. The modified stalk theory predicts that the L_α/H_{II} phase transition involves some of the same intermediate structures as membrane fusion. The small interbilayer connections observed via TRC-TEM are compatible with the structure of a critical intermediate in the modified stalk mechanism: the *trans* monolayer contact (TMC). The theory predicts that 1) TMCs should form starting at tens of degrees below T_H; 2) when TMCs become sufficiently numerous, they should aggregate into transient arrays like the quasihexagonal arrays observed here by TRC-TEM; and 3) these quasihexagonal arrays can then elongate directly into H_{II} phase domains. These predictions rationalize the principal features of our data, which are incompatible with the other transition mechanisms proposed to date. Thus these results support the modified stalk mechanism for both membrane fusion and the L_α/H_{II} phase transition. We also discuss some implications of the modified stalk theory for fusion in protein-containing systems. Specifically, we point out that recent data on the effects of hydrophobic peptides and viral fusion peptides on lipid phase behavior are consistent with an effect of the peptides on TMC stability.

INTRODUCTION

The transition between L_α and H_{II} phases involves a drastic change in the topology of the lipid-water interfaces: the system must transform from a stack of flat bilayer membranes into a hexagonally packed array of tubes with monolayer walls. The first step in the L_α/H_{II} phase transition appears to be formation of small connections between apposed bilayer interfaces (~10 nm or less in diameter), although the exact structure of these first connections has not been firmly established (e.g., Hui et al., 1983; Verkleij, 1984; Siegel et al., 1994). The initial connections between pairs of bilayers must then somehow form domains of H_{II} tubes. It has been proposed that individual connections (Hui et al., 1993; Caffrey, 1985) or pairs of connections (Siegel, 1986a) elongate directly into structures corresponding to fragments of H_{II} tubes, which then assemble sideways into H_{II} phase domains. However, despite extensive studies via freeze-fracture (e.g., Verkleij et al., 1980; Van Venetië and Verkleij, 1981, Hui et al., 1983) and cryoelectron microscopy (Frederik et al., 1989, 1991; Siegel et al., 1989b, 1994), there is not conclusive evidence for these transition mechanisms.

The first step in the process of membrane fusion must be similar to the first step in the L_α/H_{II} phase transition: small connections must also form between apposed membranes in this process, and subsequently convert into fusion pores. The structure of the first intermediates in membrane fusion has been predicted on the basis of minimization of the intermediate energies (Markin et al., 1984; Siegel, 1993). In general, for uncharged lipid systems, the lowest-energy structure for the initial connections between membranes is predicted to be that of the "stalk" (Markin et al., 1984), which is thought to transform into a hemifusion intermediate (also called a *trans* monolayer contact, or TMC; Siegel, 1993). Stalks and hemifusion intermediates have also been proposed as intermediates in protein-mediated fusion events (e.g., Chernomordik et al., 1995a, b). Therefore, one expects that the initial structures in both lipid membrane fusion and the L_α/H_{II} phase transition would be the same lowest-energy

Received for publication 9 June 1997 and in final form 16 September 1997.

Address reprint requests to Dr. David Paul Siegel, Miami Valley Labs, Procter & Gamble Co., P.O. Box 538707, Cincinnati, OH 45253-8707. Tel.: 513-627-2758; Fax: 513-627-1259; E-mail: siegel.dp1@pg.com.

Abbreviations used: L_α, liquid crystalline (lamellar) phase; cryo-TEM, cryotransmission electron microscopy; DiPoPE, (1,2-di-[C16:1 Δ9]-dipalmitoleoylphosphatidyl-ethanolamine; DOPE, dioleoylphosphatidylethanolamine; DOPE-Me, *N*-monomethylated dioleoylphosphatidylethanolamine; DSC, differential scanning calorimetry; EDTA, ethylenediamine tetraacetic acid; H_{II}, inverted hexagonal phase; ILA, interlamellar attachment (see Fig. 6 *D*); LUV, large unilamellar vesicle; MLV, multilamellar vesicle; NMR, nuclear magnetic resonance; ^{31}P-NMR; phosphorous nuclear magnetic resonance; PC, phosphatidylcholine; PE, phosphatidylethanolamine; Q_{II}, inverted cubic phase; TES, *N*-tris[hydroxymethyl]methyl-2-aminoethanesulfonic acid; T_H, equilibrium L_α-H_{II} phase transition temperature; TMC, *trans* monolayer contact (see Fig. 6 *C*); TRC-TEM, time-resolved cryo transmission electron microscopy.

0006-3495/97/12/3089/23 $2.00

structure. We can test our models of the intermediates in both processes by determining if the models are consistent with observed transition behavior.

In the present work, we used TRC-TEM to study the structure of intermediates in the L_α/H_{II} phase transition in DiPoPE as a function of temperature. The transition appears to proceed via formation of many intermembrane connections, which subsequently aggregate within the planes of the apposed bilayers to form extended arrays. These arrays have quasihexagonal symmetry in some projections, allowing them to elongate directly into H_{II} phase domains at temperatures at or above the T_H. We show that these observations are not compatible with previous theories of the L_α/H_{II} phase transition mechanism (Hui et al., 1993; Caffrey, 1985; Siegel, 1986a). However, the modified stalk theory (Siegel, 1993; submitted for publication, 1997) rationalizes the major features of these observations. Thus, our results support the modified stalk theory of intermembrane intermediates and membrane fusion. A more detailed theory of lamellar/inverted phase transitions and membrane fusion based on these results is described elsewhere (Siegel, submitted for publication, 1997).

MATERIALS AND METHODS

Materials

DiPoPE was obtained from Avanti Polar Lipids (Alabaster, AL) and was used without further purification. All other chemicals were reagent grade. Solutions were made using deionized water that was further purified with a Milli-Q Plus system (Millipore Corp., Bedford, MA).

LUVs

For TRC-TEM, dispersions of DiPoPE LUVs were produced by high-pressure extrusion using a high-pressure extruder (Lipex Biomembranes, Vancouver, BC). As with other PEs (e.g., Ellens et al., 1986, 1989), LUVs of DiPoPE can be prepared at pH 9.6. At this pH, the amine of the head group is largely deprotonated, the lipid is charged, the vesicles cannot aggregate, and the lipid cannot form the H_{II} phase. Lyophilized DiPoPE was hydrated in ice-cold 150 mM NaCl, 20 mM glycine (pH 9.6), 0.1 mM EDTA, to a final concentration of 1–1.5 mg DiPoPE/ml. The dispersions were incubated on ice for 1 h with occasional vigorous vortex-mixing, and then subjected to three freeze/thaw cycles (by immersing the flask in dry ice or liquid nitrogen, and then in room temperature water). Finally, the dispersions were then extruded 10 times through two 0.1-μm filters (Nucleopore Corp., Pleasanton, CA), using a nitrogen gas pressure of 250 ± 50 psi. For DSC and NMR, LUVs were produced using a very similar protocol, except that the lipid concentrations were higher (25 mg/ml for DSC, 50 mg/ml for NMR).

In pH-jump experiments (TRC-TEM, DSC, NMR), interactions between LUVs were triggered by rapidly dropping the pH to ~5. At this pH the LUVs can aggregate rapidly, and form H_{II} phase when the temperature is $\geq T_H$. In this study, the pH drop was achieved by mixing the lipid suspension with an acetate/acetic acid buffer at pH 4.5. Acetic acid rapidly crosses PE bilayers (Walter and Gutknecht, 1984). Under our conditions, it can be shown that enough acetic acid to neutralize the PE in the interior leaflet of the LUVs crossed the vesicle walls in ~5 ms after mixing. It is also well known that PE LUVs leak rapidly after acidification, probably through aggregation-dependent processes, and that the rate of leakage accelerates as the temperature approaches T_H (e.g., Ellens et al., 1985, 1986). Our TRC-TEM data show that the extent of nonlamellar intermediate formation also increases with increasing temperature. Therefore, the morphology we observe is not produced by residual transmembrane pH gradients.

TRC-TEM

Cryo-TEM specimens were prepared in a temperature-controlled environment at high relative humidity (Bellare et al., 1988). The temperature was accurate to within 1°C. In each experiment, 3.5–5 μl of the LUV suspension was applied to electron microscope grids covered with lacy carbon films (Ted Pella, Inc.) using a micropipette. Volumes were accurate to within ±0.1 μl. Then the same volume of pH jump buffer (100 mM NaCl, 50 mM acetate, pH 4.5, 0.1 mM EDTA) was mixed with the DiPoPE dispersion on the grid to yield a pH of 5. In separate experiments, we verified that mixing equal volumes of the glycine and acetate buffers yields a final pH of 5, and that a pH of 5.3 is obtained even when the volume of acetate buffer is 28% lower than that of the glycine, confirming that this procedure yields a reliable pH jump. The mixture was immediately blotted to form a thin film, and vitrified in liquid ethane as before (Siegel et al., 1989b, 1994; Talmon et al., 1990). The time between mixing and vitrification was typically 6–10 s. In some experiments, specimens were temperature-jumped 8–10 ms before vitrification using the flashtube system described in Siegel et al. (1994). Specimens had to be vitrified shortly after acidification because the pH jump triggered rapid aggregation of the lipid in the sample: if the aggregates grew too large, the aqueous films in the resulting cryo-TEM specimens were too thick to observe (i.e., more than several tenths of microns thick). This was especially true of specimens made at room temperature and above, and prohibited us from studying the evolution of morphology in pH-jumped specimens more than 10 s after acidification. Vitrified specimens were transferred under liquid nitrogen to a Gatan 626 cold stage and examined at −170°C in a Philips CM 12 transmission electron microscope, using 70 or 100 μm objective apertures, an accelerating voltage of 100 kV, and a set defocus of −1.8 μm. An underfocus of 1.8 μm corresponds to a first zero in the contrast transfer function of 2.5–3 nm. In practice, the true underfocus varied from micrograph to micrograph. This is due to the nonplanarity of cryo-TEM specimens (Booy and Pawley, 1993), which results in small focus errors between the area of the specimen used for setting focus and the area that is actually exposed in the low-dose mode (5 μm away in the specimen plane under the conditions used). Images obtained under these conditions showed no apparent electron beam damage to the lipid-water structures, and usually showed no damage to the polymer support films of the specimens, which are damaged at lower doses than lipid structures. Images were recorded on Kodak SO-163 film (Eastman Kodak Co., Rochester, NY) and were developed for 12 min in undiluted Kodak D-19 developed for highest electron speed.

The following control experiments were performed to verify that impurities on the EM grids did not affect the DiPoPE morphology observed via cryo-TEM. Grids were either 1) washed twice with glycine buffer, then twice with acetate buffer, then twice with Milli-Q Plus water, and dried before use; or 2) rinsed in acetone, then in chloroform (rinse, followed by a 1-h soak and another rinse in fresh chloroform), then in acetone again, then rinsed with Milli-Q Plus water (applied to the grid and blotted away four times), and finally rinsed in acetone. Similar results were obtained using both untreated grids and grids treated with either of the two protocols listed above (data not shown). In addition, we checked the effects of the two major constituents of the lacy film supports on the EM grids, Formvar and graphite, on T_H of DiPoPE, using DSC and ^{31}P-NMR; respectively (see below). We stirred acetate buffer with 1 wt % Formvar resin powder, separated the Formvar by centrifugation, used the supernatant solution to hydrate DiPoPE, and determined T_H via DSC. The same value of T_H (to within 1°C) was obtained as for DiPoPE hydrated in our normal buffer (data not shown). DSC on DiPoPE samples incubated with a small amount of graphite (99.9995% pure, from Johnson Matthey Co., Ward Hill, MA, present at a few percent of the lipid weight) also yielded the same T_H via DSC. DiPoPE incubated with a few weight percent graphite also showed only lamellar phase ^{31}P-NMR patterns at 35°C (data not shown). As

determined by DSC, 35° is below T_H, but is a temperature at which abundant intermediate morphology was observed via cryo-TEM (see Results and Discussion). Therefore, impurities from the lacy films are not responsible for the nonlamellar morphologies observed at $T < T_H$ via cryo-TEM.

DSC methods

DiPoPE LUV dispersion (0.8 ml) at pH 9.6 (25 mg/ml) was introduced into the sample cell of a MicroCal MC-2 DSC (MicroCal Inc., Northampton, MA), allowed to thermally equilibrate at the experimental temperature (between 0 and 35°), and then mixed with 1.0 ml of acetate pH-jump buffer at approximately the same temperature. When the temperature stabilized, the scan was begun at a rate of 19 K/h.

NMR methods

^{31}P-NMR spectra were also obtained from DiPoPE LUV dispersions acidified at various temperatures below T_H. DiPoPE LUV dispersions were acidified with acetate buffer in NMR tubes at the experimental temperatures just as for the DSC experiments, above, except that the DiPoPE concentration was twice as high. Samples were then immediately inserted into the spectrometer. Spectra were obtained in either a Bruker AC-300 or Bruker Avance DRX-500, using a flip angle of 90°, delay times of 0.25 (AC-300) or 0.5 s (DRX-500), acquisition times of 0.43 (AC-300) or 0.34 s (DRX-500), and line broadening of 100 Hz.

X-ray diffraction

DiPoPE was hydrated in buffer (150 mM NaCl, 20 mM TES (pH 7.4), 0.1 mM EDTA) at a lipid concentration of 33 wt % at 4°C, and allowed to equilibrate for 1 h at that temperature. The suspension was freeze/thawed three times (dry ice/30°C water bath) and then loaded into x-ray capillaries. The sample tended to separate into a white lipid fraction and excess buffer. To ensure complete hydration, a weight of buffer roughly equal to the weight of the lipid-rich fraction was added to each capillary. The capillaries were flame-sealed and stored overnight at 4°C. Separate capillaries were preincubated at 39°C or at 41.5°C for 2 h, and then exposed in the x-ray beam for 2½-3 h (Rigaku RH100 rotating-anode x-ray generator with a flat-film camera and a sample-to-film distance of 30 cm).

RESULTS

Phase behavior of DiPoPE

The L_α-to-H_{II} phase transition was studied using DiPoPE because it has an experimentally convenient T_H of 43°C, as determined by DSC (Epand, 1990). Moreover, DiPoPE does not form detectable amounts of Q_{II} phases when heated through T_H. An earlier TRC-TEM study of the intermediates in L_α-to-H_{II} phase transitions (Siegel et al., 1994) was done using DOPE-Me. DOPE-Me can form Q_{II} phases in parallel with H_{II} phases (Siegel and Banschbach, 1990) at temperatures near T_H. This led to some ambiguity about assignments of intermediate structure to either the L_α/H_{II} or L_α/Q_{II} phase transition mechanisms (see Discussion). The evidence that DiPoPE doesn't form Q_{II} phase comes from x-ray diffraction studies of samples incubated briefly at temperatures near T_H (Colotto et al., 1996; Colotto and Epand, 1997). In the present work, this was also checked using samples incubated in excess buffer for several hours at temperatures just below T_H (see Materials and Methods). DOPE-Me samples treated in this way yield intense Q_{II} phase reflections (Siegel and Banschbach, 1990). In contrast, DiPoPE dispersions incubated for several hours at 39° or 41.5°C yielded diffraction patterns showing the presence only of a lamellar phase (layer spacing of 4.75 ± 0.1 nm) at 39°C and of L_α and H_{II} phases (H_{II} tube diameter of 7.0 ± 0.1 nm) at 41.5°C, although there was a very weak trace of a reflection at 17 nm for the 39° sample (data not shown). These results confirm that DiPoPE forms very little, if any, Q_{II} phase under the conditions of this study, and that the intermediate morphology that we observed represents intermediates in the L_α/H_{II} phase transition.

TRC-TEM images of DiPoPE LUV suspensions

Fig 1*A* is a micrograph of DiPoPE LUVs at pH 9.6. As expected, the lipid was present mostly as unilamellar vesicles roughly 0.1 μm in diameter. The dark bands in this and other micrographs are strands of a lacy carbon-coated polymer support that promotes aqueous film formation on the electron microscope grids. The dark, irregularly shaped particles are tiny bits of frost adsorbed on the vitrified specimen from the liquid nitrogen. Fig. 1 *B* is a micrograph of a pH-jumped suspension vitrified from a temperature of 5°C. The LUVs have clearly aggregated, and strongly adhere to one another, as evidenced by the distortion of the vesicles within the aggregates (*lower right*). Formation of a small multilamellar structure is obvious in the upper left-hand corner. Similar morphology was previously observed for egg PE LUVs at low pH (Siegel et al., 1994), and is consistent with low pH-induced aggregation and rupture of PE LUVs (e.g., Ellens et al., 1985, 1986, 1989).

In micrographs obtained at higher temperatures, aggregation is much further advanced, and qualitatively new types of structures are visible. Fig. 1 *C* shows a suspension pH-jumped at 21°C. The presence of multilamellar structures several tenths of microns in diameter shows that extensive aggregation and rearrangement of the original LUVs has taken place. The small arrows indicate regions in which many small connections have formed between apposed bilayers. Note that these occur in clusters, but that the clusters do not seem to have any long-range order. The hollow arrows and arrowheads indicate another type of structure. The hollow arrows mark regions where there are series of dark striations spaced ~7–7.5 nm apart. These regions frequently abut regions where there are hexagonally packed arrays of circles ~8–9 nm in diameter (*arrowheads*). Because these two types of features are always seen in conjunction (Fig. 1, *C–F*), it is assumed that they represent two different views of the same or related structures. We refer to such domains as quasihexagonal domains. Note that although these quasihexagonal domains resemble the expected appearance of H_{II} phases in cryo-TEM (domains of H_{II} tubes seen from the side and along the axis of the tubes, respectively), the sample was acidified at a temperature 22° *below* T_H. Finally, the asterisks indicate structures

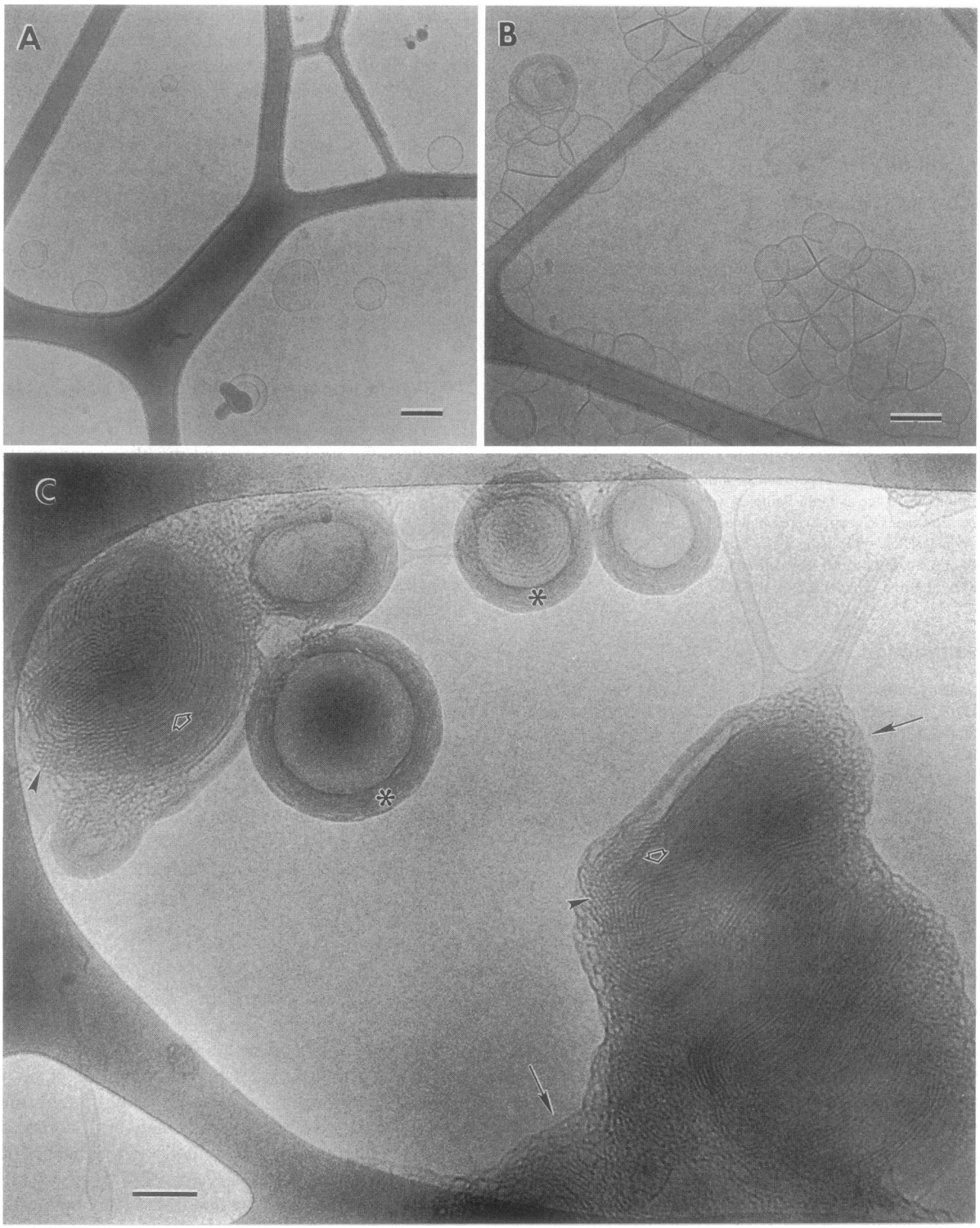

FIGURE 1 TRC-TEM images of DiPoPE LUV dispersions. (*A*) DiPoPE LUVs at pH 9.6 and room temperature. (*B*) DiPoPE LUVs after acidification to pH 5 at 5°C. (*C*) pH 5, 22°C (i.e., 21 K below T_H). *Solid arrows:* clusters of intermembrane connections. *Hollow arrows:* lattices of dark striations. *Arrowheads:* regions of hexagonal symmetry. The striations and hexagonal symmetry are always associated, and termed quasihexagonal domains. *Asterisks:* MLVs. The interbilayer water spacings are too small to be clearly resolved under these focal conditions (see Fig. 3 *C*). All symbols have the same meaning in *C–F*. (*D*) pH 5, 26°C (16 K below T_H). Note the circular profiles making up the hexagonal lattice, and the bilayer structure of the striations. (*E*) pH 5, 31°C (12 K below T_H). The relative abundance of quasihexagonal morphology increases with temperature. (*F*) Specimen acidified to pH 5 at 35°C, and then temperature-jumped to $T \approx 80$°C 10 ms before vitrification. The lipid aggregates are denser, and the hexagonal lattice spacing is close to that of the H_{II} phase. (*G*) pH 5, 5°C (same conditions as in (*B*)). Clusters of intermembrane connections and quasihexagonal-like structures were infrequently observed in specimens made at low temperatures. However, the morphology in (*B*) is more representative of specimens made under these conditions. Scale bars = 100 nm in all cases.

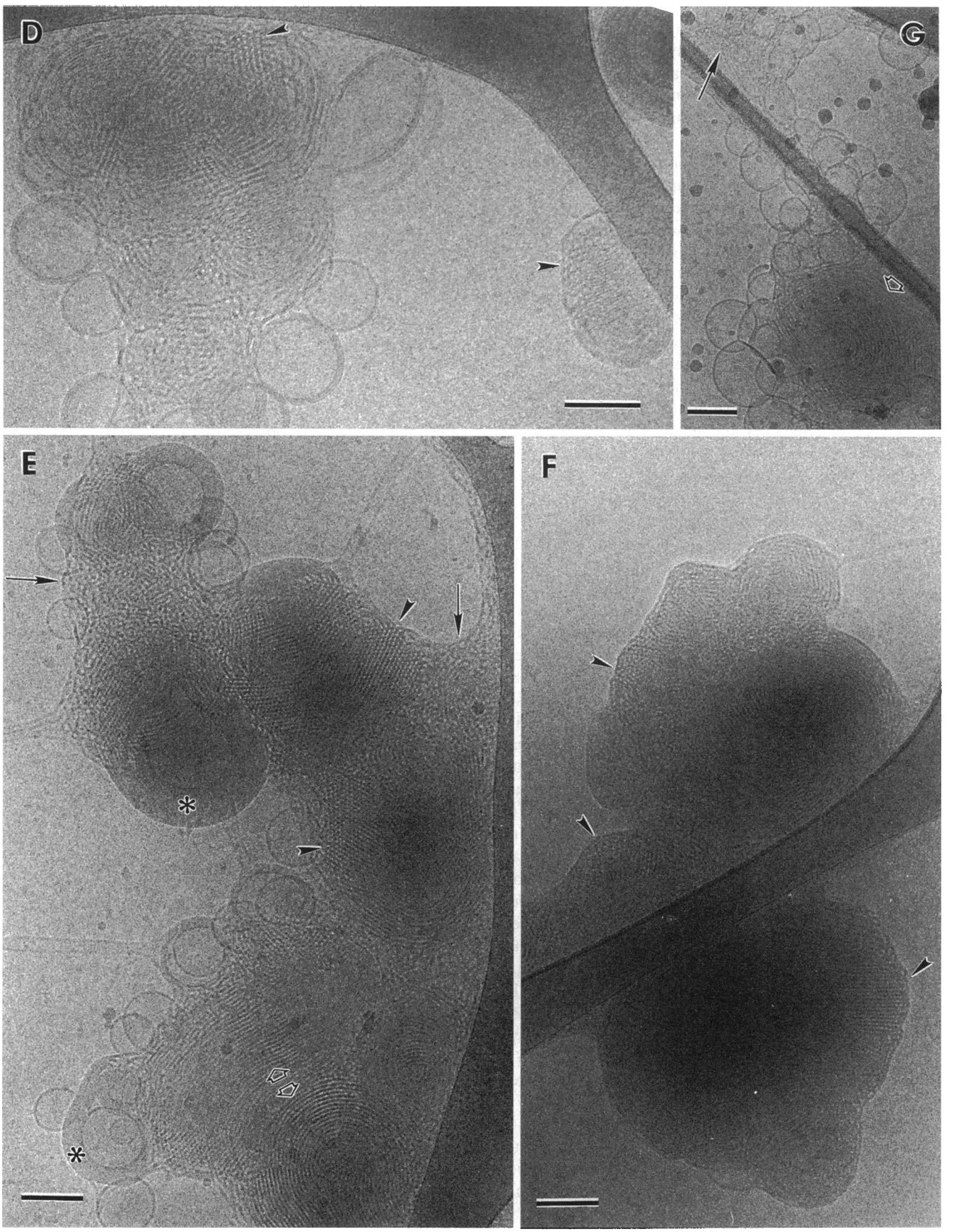

Figure 1 *Continued.*

that are clearly small MLVs, which are small domains of the equilibrium L_α phase. The water layers between bilayers in the L_α phase are thought to be only ~0.5 nm thick in PEs (McIntosh and Simon, 1996), so that the individual bilayers are just barely resolved. The presence of MLVs shows that they are being produced in parallel with, or from, the quasihexagonal structure.

Fig. 1 *D* is a higher magnification image of quasihexagonal domains in a specimen pH-jumped at 26°C. The arrowheads mark regions where circular profiles are seen in a hexagonal array. This micrograph was taken closer to focus than Fig. 1 *B*, and more clearly shows the circular shapes of the hexagonally packed profiles (which are ~8.5 nm in diameter). This is important because it shows that the hexagonally packed structure is not a Moiré pattern-like illusion created by the superposition of two arrays of bilayers oriented at different angles. (Also, see the discussion of Fig. 3 below.) This image also shows that the striations have a bilayer cross-section (two headgroup planes per layer). Fig. 1 *E* shows a specimen pH-jumped at 31°C (12° below T_H), showing that the number and extent of the quasihexagonal domains increase with increasing temperature. The symbols are the same as in Fig. 1 *C*.

Fig. 1 *F* shows a dispersion that was pH-jumped at 35°C (8° below T_H), and subsequently temperature-jumped to ~80°C (well above T_H) at a time ~10 ms before vitrification, using the flashtube apparatus described by Siegel et al. (1994). Specimens subjected to this procedure were very thick due to rapid growth of the lipid aggregates. Few regions of the specimen films were thin enough to observe via cryo-TEM. The aggregates in Fig. 1 *F* are denser than in *C–E*, and are too thick to reveal the fine structure of most of the lipid. However, the fine structure of lipid at the periphery of the aggregates is visible, and resembles the quasihexagonal morphology observed at lower temperatures (e.g., the hexagonal packing indicated by the arrowheads, with an apparent tube diameter of 7 nm). The major differences in appearance between Fig. 1 *F* and *C–E* are that nearly all the unilamellar vesicles are absent in *F*, that a larger fraction of the lipid is present as the quasihexagonal structure and/or domains of H_{II} phase, and that the diameter of the circular profiles are smaller than at lower temperatures. It is likely that there were domains of H_{II} phase present in the aggregates in *F*. The specimen was temperature-jumped well above T_H for a time long enough to allow extensive conversion to the H_{II} phase, as determined from an earlier study of egg PE (Siegel et al., 1994). Moreover, the diameter of the circular profiles in Fig. 1 *F* is close to the diameter expected for H_{II} phase at around T_H. This suggests that domains of quasihexagonal structure formed below T_H can rapidly grow into H_{II} domains at $T > T_H$.

There appeared to be no well-defined onset temperature for formation of the clusters of intermembrane connections and the quasihexagonal structure. Data from more than 22 experiments show that such morphology is rarely observed at 5°C, is usually observed at 21–27°C, and is always present at 31–34°C. Fig. 1 *G* shows examples of a cluster of intermembrane connections (*arrow*) and a small domain of what may be quasihexagonal structure (*hollow arrow*) in a specimen prepared at 5°C. Note that the domain of quasihexagonal structure in this case lacks the circular profiles seen at higher temperatures (Fig. 1, *C–F*), but has about the same large interlamellar spacing (~7.5 nm) as seen at higher temperatures; much larger than the equilibrium lamellar phase spacing of ~4.75 nm. There may be no well-defined onset temperature for formation of the clusters and quasihexagonal domains because of temperature-dependent differences in LUV aggregation rates. Extensive LUV aggregation is necessary before the quasihexagonal structures can form (Fig. 1, *C–F*), and LUV aggregation may be slower at low temperatures. For roughly the same mixing-to-vitrification interval, aggregation is less extensive when the specimens are made at lower temperatures (compare Fig. 1 *B* with *E*). Moreover, the mixing-to-vitrification interval varied by a few seconds between specimens, so that the aggregation conditions were never perfectly reproducible. We consistently observe that the proportion of quasihexagonal structure to intermediate cluster structure increases with increasing temperature. It is not clear whether this reflects a temperature-dependent increase in a steady-state ratio of the two types of structure, or an increase in conversion rate to the quasihexagonal structure. A time course study at a single temperature could determine this, but we were unable to do this for the reasons given in Materials and Methods.

Images of specimens pH-jumped at 2°C and subsequently temperature-jumped above T_H 10 ms before vitrification showed clusters of intermembrane connections and quasihexagonal domains nearly as extensive as for specimens pH-jumped and vitrified from 26 to 31°C (data not shown). This shows that extensive intermembrane connections and quasihexagonal domains can form within milliseconds upon an increase in temperature.

Fine structure of the clusters of intermembrane connections

These clusters are presumed to precede formation of quasihexagonal domains because they predominate at lower temperatures, and are often seen in smaller lipid aggregates, than the quasihexagonal domains. It is notable that connections between membranes are not seen in isolation. They occur in regions where the LUV aggregation process is far advanced, and are not obvious between LUVs that are not tightly apposed. This suggests that formation of the first intermembrane structures is cooperative, or that formation is rapid once proper conditions (e.g., close apposition) are achieved, or that the isolated intermediates aggregate immediately after formation. Presently, it is not possible to resolve the structural elements of the clusters via cryo-TEM, due to the superposition of many elements in each projection (e.g., Fig. 1, *C–F*), and due to the limited contrast generated by the high-curvature segments of monolayers

and bilayers involved. This latter point was demonstrated by Siegel et al. (1994): at focal conditions permitting resolution of the monolayer leaflets of DOPE-Me bilayers, bilayers bent into radii of curvature of the same size as small unilamellar vesicles were nearly invisible. This indicates that individual intermediate structures (diameters of 10 nm or less) would be nearly invisible under the relevant range of focus conditions.

The early intermediate morphology in DiPoPE is compared with the same morphology in temperature-jumped DOPE-Me specimens (Siegel et al., 1994) in Fig. 2. The micrograph on the left shows a cluster of intermediates in a specimen of pH-jumped DiPoPE prepared at 31°C. At right is an image (same magnification) of an LUV dispersion of DOPE-Me temperature-jumped to a temperature some 25° above T_H ~9 ms before vitrification. Three differences are immediately apparent. First, the density of intermembrane connections is much larger, and the original LUVs have much more extensively aggregated and rearranged in DiPoPE, even though DiPoPE is 11° below T_H under these conditions. This may reflect 1) the stronger repulsive short-range forces between monomethylated PE bilayers compared to PE (Rand et al., 1988), which would slow down LUV aggregation and intermembrane contact formation; and 2) the briefer interval for LUV aggregation available to the DOPE-Me specimen. Second, the DOPE-Me contains large well-defined interlamellar attachments (ILAs, or fusion pores; indicated by arrowheads), which are absent in DiPoPE. The arrowheads indicate ILAs (catenoidal bilayer connections between apposed lamellae) as viewed from the side. The outside diameter of the ILAs is ~15 nm at the narrowest point (although there is variation of several nm in this dimension), and the "height" of ILAs is approximately the same. ILAs viewed along their axes appear as circles (Siegel et al., 1989b), which may correspond to the profiles indicated by the arrow in the DOPE-Me micrograph. Third, the clusters of intermediates in DiPoPE appear to contain circular or nearly circular profiles of a smaller diameter, as well as short line segments. These views represent projections of many superimposed elements without long-range order. It is therefore not possible to determine the structural elements of the cluster. However, it is clear that the characteristic length scale of the intermediates in DiPoPE is much smaller (e.g., "diameter" of profiles of 10 nm or less, separation of bilayer interfaces of ~4 nm) than in DOPE-Me.

The DiPoPE morphology in Fig. 2 probably does not represent a dense array of ILAs, for four reasons. First, there are no clear examples of side views of ILA structure as in

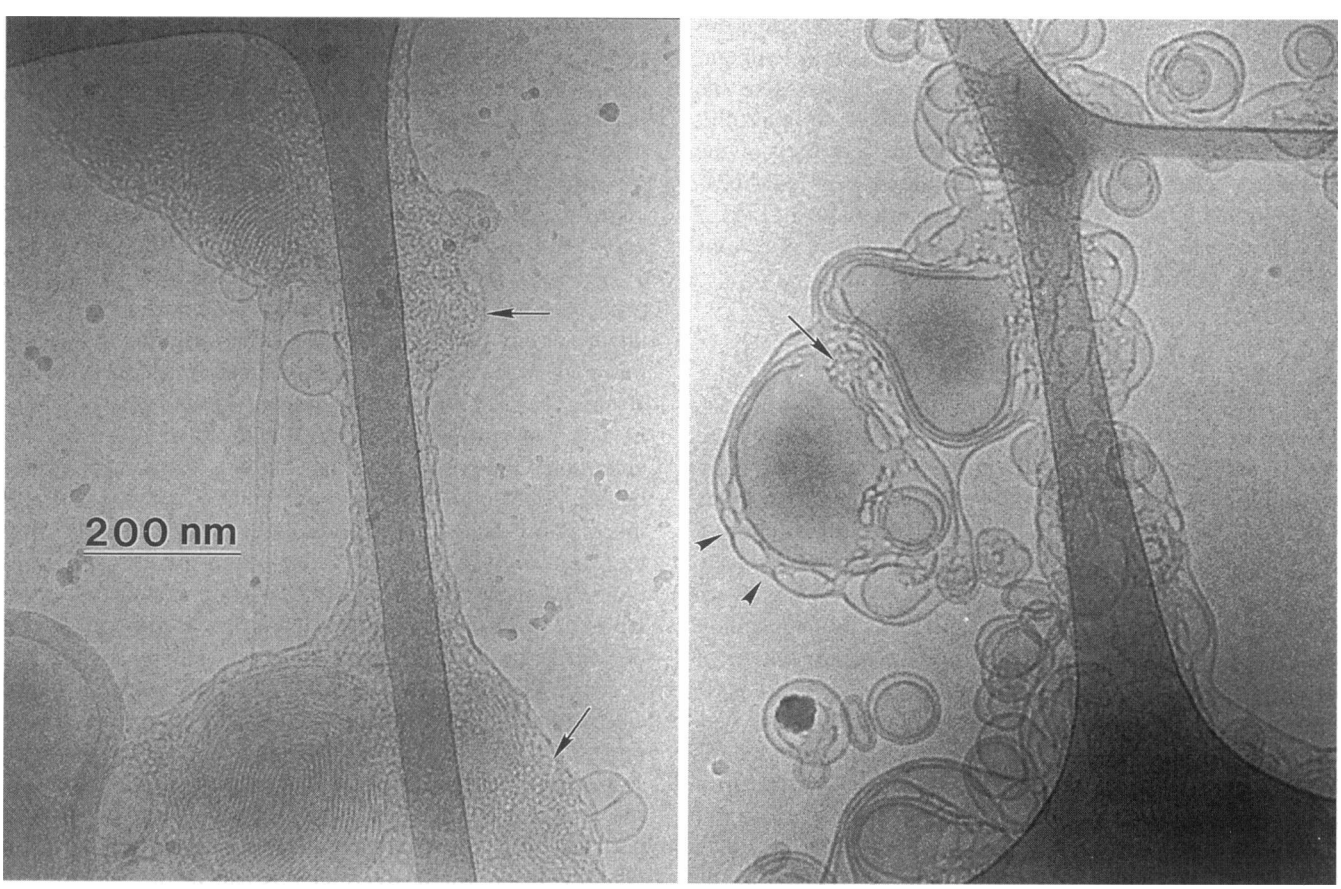

FIGURE 2 Comparison of intermediate morphology in DiPoPE and DOPE-Me (Siegel et al., 1994), at the same magnification. Left: DiPoPE LUVs acidified to pH 5 at 31°C. *Arrows:* i clusters of intermembrane connections. Right: DOPE-Me LUVs temperature-jumped to ~25° above T_H ~10 ms before vitrification. *Arrowheads:* ILAs as seen from the side. *Arrows* indicate ILAs viewed down their axes. Scale bar = 200 nm.

DOPE-Me. Second, the apparent circular profiles in DiPoPE are considerably smaller than the diameter of the ILAs in DOPE-Me, and this difference is too large to be explained by a difference in spontaneous curvature between the two lipids. The diameter of H_{II} tubes in DOPE-Me and DiPoPE at their respective values of T_H is similar: 7 nm for DiPoPE (present study; Colotto et al., 1996; Colotto and Epand, 1997) versus 7.4 nm for DOPE-Me (Gruner et al., 1988). This indicates that the difference in spontaneous curvature between the two lipids is small (<0.4 nm, considering the difference in monolayer thickness). Third, ILAs are intermediates in the L_α/Q_{II} phase transition (Siegel, 1986b; Ellens et al., 1989; Siegel et al., 1989b); a transition that DiPoPE does not execute spontaneously, while DOPE-Me does (Siegel and Banschbach, 1990). Fourth, ILAs are very long-lived structures in PE and PE analogs, and only revert to bilayer structure if the lipid suspension is frozen to temperatures below the chain melting temperature of the lipid (Gagné et al., 1985; Ellens et al., 1986, 1989; Gruner et al., 1988). Therefore, if the numerous structures seen in DiPoPE were ILAs, we would expect to see a prominent and long-lived isotropic resonance in ^{31}P-NMR spectra of these dispersions. As will be shown below, this was not observed.

Interestingly, some of the morphology observed for DOPE-Me transition intermediates is reminiscent of the intermembrane connection clusters and quasihexagonal domains in DiPoPE. The larger lipid aggregates in temperature-jumped DOPE-Me seem to contain regions like the clusters of intermembrane connections seen in DiPoPE, with ILAs forming predominantly at the periphery of the aggregate, and small inclusions of what may be quasihexagonal domains are visible in some specimens (e.g., Figs. 7 and 8, respectively, of Siegel et al., 1994). The implications of this are described in the Discussion below.

Quasihexagonal structure

The major features of the quasihexagonal morphology are that in some projections the structure resembles hexagonally packed circles, and in others a series of bilayer striations with a spacing of ~7–7.5 nm. The diameter of the circular profiles is 8–9 nm at temperatures below 31°C, but appears to shrink at temperatures of 31 and above, where it is becomes ~7–7.5 nm (Fig. 1, *E* and *F*). An apparently hexagonal structure might arise from the superposition of two sets of bilayers that lay across one another at an angle of ~60°. However, this is not the origin of the observed hexagonal symmetry. As shown in Fig. 1 *D*, in some regions the hexagonal lattice consists of clearly circular profiles (*arrowheads*), which could not be produced in this manner. This is emphasized in Fig. 3 *A*, which shows a specimen prepared at 31°C. The arrowheads indicate regions at the periphery of the aggregates with clearly circular profiles. Moreover, it is difficult to imagine a type of structure that would maintain two lamellar lattices in just the correct registration across an entire aggregate, which happens frequently in our micrographs (e.g., lower left-hand corner of Fig. 3 *A*). Occasionally, we noticed regions where apparent superposition of lamellar lattices produced the appearance of a cross-hatched structure (*large arrows* in Fig. 3, *A* and *B*). However, these regions usually occur in a small fraction of the a lipid aggregate, and the angle between the layers of the two inferred lattices is often far from 60°. The overall appearance of the cross-hatched areas in these regions is quite different from the extensive arrays of circular profiles seen in Figs. 1, *C–F* and 3 *A*.

The morphology of the quasihexagonal structure is superficially similar to that of the H_{II} phase. Obviously, since this structure occurs far below equilibrium T_H, this is an unlikely explanation. In addition, the apparent unit cell size in the hexagonal projection, and the spacing of the striations of the quasihexagonal structure, are both significantly larger than expected for H_{II} phase. At temperatures of 21–27°, the apparent diameter of the hexagonally packed circular profiles is ~8–9 nm, and the striation spacing is ~7.5 nm. In comparison, the H_{II} tube diameter is ~7 nm at T_H, and the d_{10} and d_{11} spacings of the DiPoPE H_{II} phase, as determined by x-ray diffraction, are ~6.1 and 3.5 nm at T_H (data not shown). Even allowing for the small increase in H_{II} unit cell with decreasing temperature (~0.015 nm per degree for DOPE; Tate and Gruner, 1988; Kozlov et al., 1994), the dimensions of the quasihexagonal structure are significantly different from those of the H_{II} phase. However, the appearance of the quasihexagonal structure is similar enough to H_{II} phase that we explored the possibility that it actually represents an H_{II} phase that formed in our suspensions below the equilibrium T_H for some unknown reason. There is sometimes evaporation of water from thin aqueous films of cryo-TEM specimens before vitrification (Dubochet et al., 1988), and dehydration reduces T_H in many PEs. However, this could not be responsible for formation of an H_{II} phase under our circumstances. There is obviously excess water in the planes of the cryo-TEM specimens imaged in our micrographs, and the T_H of PEs is insensitive to small changes in salt concentration (Koynova and Caffrey, 1994). We entertained the possibilities that 1) there was some impurity on the microscope grids that lowered T_H for the DiPoPE dispersions; and/or 2) that H_{II} phase forms at a lower temperature in acidified LUV dispersions than in bulk multilamellar preparations, where this transition is usually studied. Therefore, we performed control experiments to test both these possibilities.

As described in Materials and Methods, when we used electron microscope grids subjected to extensive washing in both water and organic solvents, we still observed the same sort of quasihexagonal morphology (data not shown). This shows that extractable impurities from the polymer supports, if present at all, do not affect T_H of DiPoPE. We also verified that Formvar polymer (present in tiny amounts in the EM grid supports) contains no extractables that would alter the T_H. To do this, we used buffer equilibrated with Formvar powder to hydrate DiPoPE, and then determined

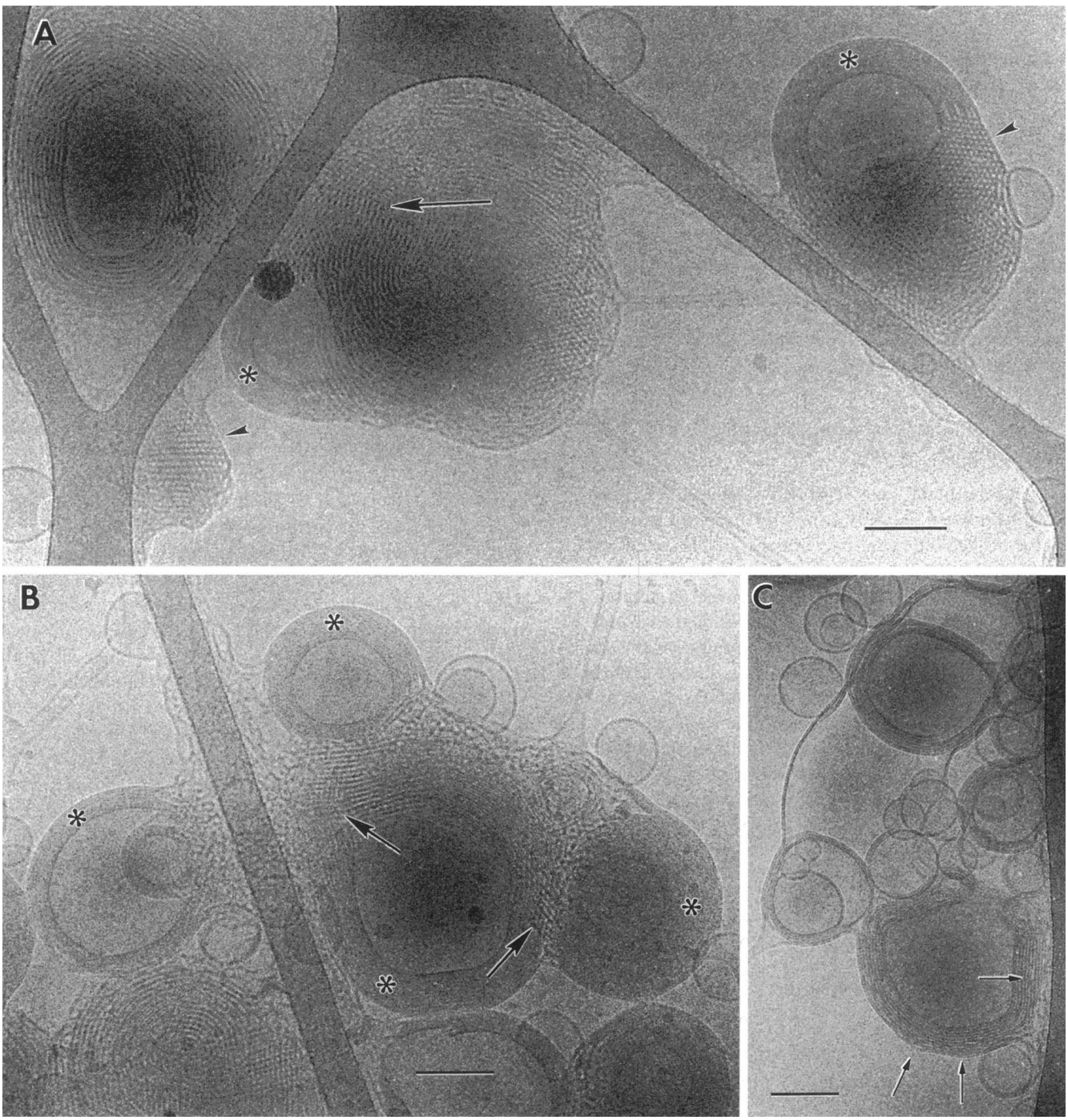

FIGURE 3 (*A* and *B*) DiPoPE LUVs at pH 5, 31°C. In both (*A*) and (*B*), *arrowheads* and *asterisks* indicate regions of hexagonal symmetry and MLVs, respectively, while the *large arrows* indicate regions where superimposed arrays of lines create an artifactual lattice. Note that the morphology in such regions is easily distinguished from the hexagonal symmetry indicated by arrowheads here and in Fig. 1. In (*B*), note that quasihexagonal domains abut onto MLVs, implying that the quasihexagonal structure can decay into MLVs. (*C*) LUVs at pH 5, 22°C. Collapse of aggregated LUVs into MLVs. *Small arrows* regions where there are local close contacts between lamellae. These seem to be in the process of expanding into the closely packed MLV structure. Scale bars = 100 nm.

T_H using DSC. The transition temperature was the same as untreated DiPoPE to within <1° (data not shown). The only other nonmetallic substance present on washed grids was graphite. Using DSC, we verified that small amounts of graphite do not change T_H (data not shown), though some lipid does adsorb tightly to the graphite powder we used. Therefore, we conclude that impurities do not significantly lower the T_H of DiPoPE, and cannot explain the abundance of H_{II}-like morphology we observed at temperatures 22° or more below T_H. Many of the micrographs give the impres-

sion that a lot of intermembrane connection clusters and quasihexagonal domain formation begins in lipid aggregates at the periphery of the holes in the lacy film supports of the EM grids, adhering to the graphite-coated strands of polymer film (e.g., Fig. 1 *C*). This is probably a result of the thinning of aqueous films before vitrification, which tends to sweep suspended material to the periphery of the films (Dubochet et al., 1988). However, because of this association of nonlamellar morphology with the graphite-coated supports, we did experiments to show that the presence of graphite/water interfaces did not catalyze H_{II} phase formation at $T < T_H$ through some obscure effect. We performed ^{31}P-NMR experiments that showed that small amounts of suspended graphite did not induce formation of H_{II} phase in acidified LUV dispersions (see the next subsection).

The quasihexagonal structure is not an equilibrium H_{II} phase

Next, we used DSC and ^{31}P-NMR to determine whether T_H is different when DiPoPE is initially dispersed as LUVs, as opposed to multilamellar preparations. In DSC experiments, we acidified DiPoPE LUV dispersions at a given temperature within the sample cell of a calorimeter equilibrated at that temperature, and then scanned the temperature upward. We reasoned that if H_{II} phase was forming at lower temperatures in acidified LUV dispersions, then the transition endotherm normally observed at 43°C in multilamellar preparations would not be present. The top trace in Fig. 4 shows an endotherm of DiPoPE multilamellar liposomes produced by direct hydration of dry lipid, showing a phase transition at 43°C. The next three traces are endotherms of DiPoPE LUVs acidified at 0, 30, and 34°C, respectively. An endotherm is present at 42–43°C in each case, though it broadens as the temperature of acidification increases. The value of T_H for LUVs acidified at 0, 30, 32.5, 34, and 35° was 42.4 ± 0.7°C, within <1°C of the value obtained for MLVs (Epand, 1990). However, the endotherms became quite broad when LUVs were acidified at temperatures above 30°C (e.g., 34°C trace in Fig. 4). On account of this, it was not possible to make accurate estimates of the transition enthalpy, which could be compared with the enthalpy of the transition in MLVs. Thus, although there is clearly lipid undergoing the L_α/H_{II} transition at the MLV value of T_H in these dispersions, the possibility that some of the lipid had undergone an L_α/H_{II} transition at the temperature of acidification was left open by these experiments. We suggest that the broadening of the endotherms in acidified LUV dispersions relative to MLVs occurs because LUV aggregation produces smaller MLVs than does hydration of dry lipid. The MLVs in Fig. 1, *C–E* and Fig. 3 are only tenths of microns in diameter, whereas MLVs obtained by direct hydration are often in the micron range. The transition should be less cooperative in the smaller MLVs.

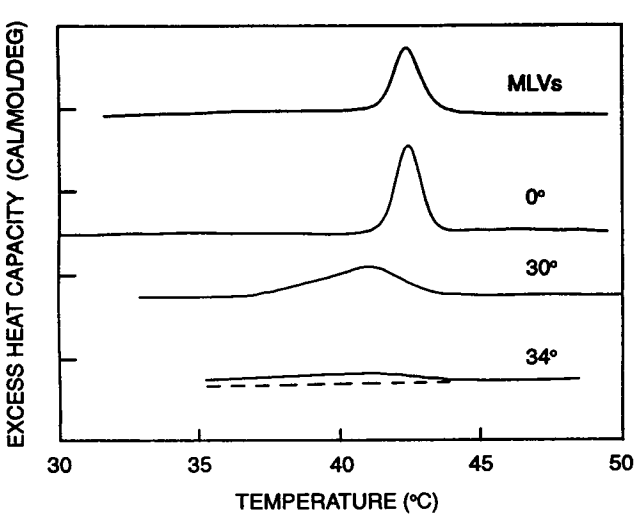

FIGURE 4 Differential scanning calorimetry thermograms of DiPoPE. *Top:* Endotherm of DiPoPE MLVs produced by direct hydration of dry lipid. The next three traces are endotherms obtained from DiPoPE LUVs acidified at 0, 30, and 34°C, respectively. Each tick mark on the ordinate corresponds to 200 cal/mol/deg.

To further explore the possibility that H_{II} phase forms at lower temperatures in acidified LUVs, we performed ^{31}P-NMR experiments on LUV dispersions acidified at temperatures below T_H. The shape of the ^{31}P-NMR resonance from phospholipid samples is a reliable indicator of the presence of inverted phases (Cullis et al., 1983). Fig. 5 *A* shows ^{31}P-NMR spectra from MLV samples of DiPoPE in the L_α phase (31°C; *bottom*) and H_{II} phase (51°C; *top*). Fig. 5 *B* shows spectra obtained from dispersions of DiPoPE LUVs. The top spectrum was obtained from a sample at pH 9.9 at 35°C. The resonance most resembles an isotropic resonance, reflecting the motional averaging produced by LUV tumbling on the NMR time scale (Cullis et al., 1983), though there is also a hint of a component more like the bulk lamellar phase. The middle and bottom spectra were obtained from an LUV dispersion acidified at 35°C and then immediately inserted into the spectrometer. The middle spectrum was integrated for 43 s, starting 1 min after acidification. The bottom spectrum was obtained from the same sample ~5 min after acidification. Both spectra are clearly lamellar phase spectra, with no detectable H_{II} phase component. Similar behavior was observed for samples acidified at 30 and 32.5°C, although in some cases the spectra initially contained small isotropic components that decayed over the interval between 5 and 15 min after acidification (data not shown). The isotropic components may be due to a small number of residual LUVs, or to lipid in longer-lived intermediate structures. Therefore, in LUVs acidified at 30–35°C, there is no H_{II} phase present 1–2 min after acidification, despite the abundance of quasihexagonal morphology seconds after acidification in this temperature range (Fig. 1, *E* and *F*; Fig. 3).

Additional ^{31}P-NMR experiments were also performed on dispersions of LUVs acidified at 34°C in the presence of 48% by lipid weight of finely divided graphite (data not shown). The results were similar to those in Fig. 5 *B*, and

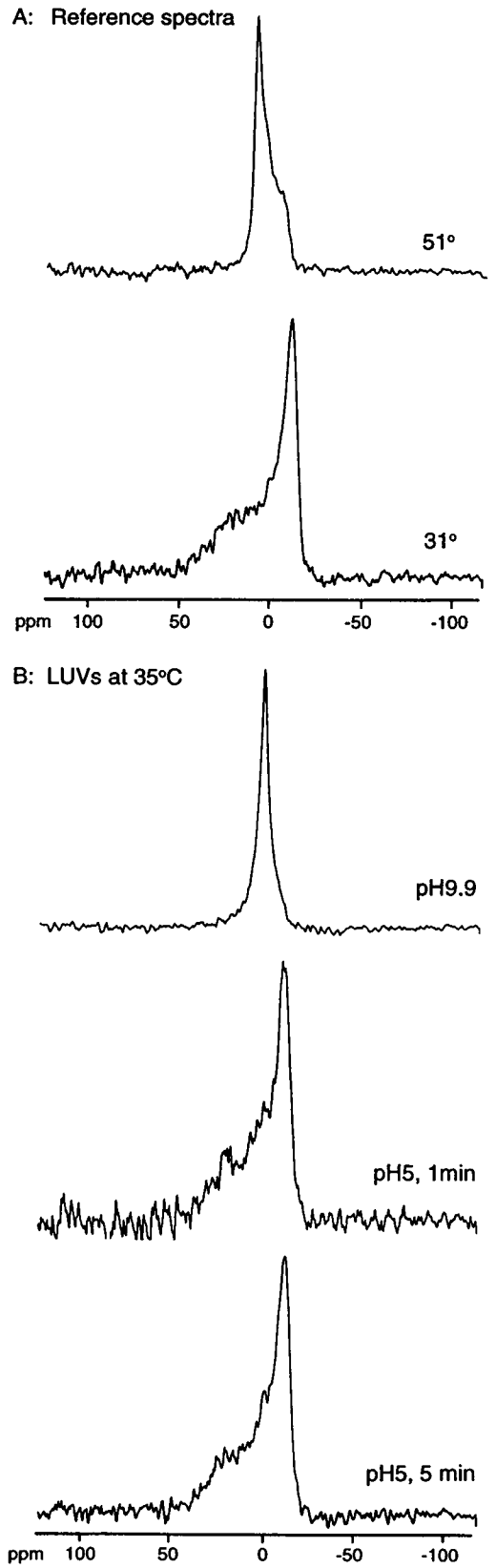

FIGURE 5 ^{31}P-NMR spectra of DiPoPE. (*A*) Spectra of MLVs at 31°C (*bottom*) and in the H_{II} phase at 51°C (*top*). (*B*) Spectra obtained from LUV dispersions at 35°C. *Top:* pH 9.6 (i.e., no acidification). *Middle:* LUVs acidified to pH 5, collected between 1 and 2 min after acidification. *Bottom*: Same sample, collected between 5 and 8 min after acidification.

show that the graphite present on EM grids is not inducing H_{II} phase formation at $T < T_H$ through some obscure effect.

Together, these results allow two important conclusions. First, the quasihexagonal structures observed via TRC-TEM do not represent an equilibrium H_{II} phase. Second, the time-resolved ^{31}P-NMR spectra indicate that the abundant nonlamellar structures observed via TRC-TEM seconds after acidification (Fig. 1, *C–F*; Fig. 3) must be absent by 1–2 min, or at most by 15 min, after acidification. The reason is that the small radii of curvature of the morphology in Fig. 1, *C–F* and Fig. 3 should generate rapid motional averaging on the NMR time scale due to diffusion of lipids around the lipid-water interfaces. If the specimen contained as large a fraction of quasihexagonal structure as evidenced in the micrographs, one would expect to see a substantial nonlamellar component in the ^{31}P-NMR spectra. These are clearly absent after ~1–2 min in Fig. 5 *B* (although a small isotropic component was sometimes observed after 1–2 min, which represented 10% or less of the total intensity, and which decayed within 5–15 min). Thus, the nonlamellar morphology observed via cryo-TEM is transient, with a lifetime of minutes or less. These results leave open the possibility that the quasihexagonal structure is some sort of transient, nonequilibrium H_{II} phase, but we cannot at present understand what would drive the L_α/H_{II} phase transition below the equilibrium T_H, and then cause it to reverse itself. In the Discussion, we present what we think is a much more compelling rationale for these results.

MLVs form from or in parallel with quasihexagonal structures in acidified LUV dispersions

Formation of MLVs occurs on the same time scale as formation of the intermembrane connection clusters and quasihexagonal domains in acidified LUVs. For example, small MLVs are visible in Fig. 1, *C* and *E*, and Fig. 3. A micrograph of a specimen acidified at 31°C is shown in Fig. 3 *B*. This image emphasizes that MLVs are seen adjoining regions of quasihexagonal domains and clusters of intermembrane connections, implying that there is a route by which MLVs may interconvert with these structures. Since the MLVs are domains of L_α phase, the equilibrium phase under these conditions, and since the nonlamellar structures are occasionally seen in lipid aggregates that have not formed MLVs, the MLVs presumably form either from, or in parallel with, the nonlamellar morphology. Fig. 3 *C* is a micrograph of a specimen acidified at 21°C. At this lower temperature, nonlamellar structures made up a smaller fraction of the lipid in the samples. Note that at several locations within the multilamellar aggregates (*small arrows*), the local water layer thickness between lamellae is larger than in the most ordered regions, and that there are what appear to be local adhesions of the lamellae within these larger-spacing regions. We assume that this represents an intermediate stage in formation of MLVs from LUVs, in which

disruption of aggregated LUVs forms loose concentric shells of bilayers, which then adhere at foci, followed by focal contact expansion, which closely apposes as much bilayer-bilayer interface as possible. The overall process is probably driven by the large energy of mutual adhesion of PE bilayers at pH 7 or less (McIntosh and Simon, 1996). This shows that there is also a direct pathway between LUVs and MLVs under these circumstances, involving no widespread formation of nonlamellar intermediates.

DISCUSSION

The most striking aspects of our results are as follows.

1. The first intermembrane connections that we observe are small (~10 nm in diameter), and are seen in large clusters seconds after acidification (Fig. 1, *B–E*; Fig. 2). These clusters contain high densities of intermediates, can be 0.1 μm or more in diameter, but have no long-range order. They are common in specimens acidified at 22° below T_H, and abundant at higher temperatures. Smaller clusters of intermediates are infrequently observed at 38° below T_H.
2. These intermediates appear to transform into a structure with long-range order, which we refer to as quasihexagonal domains. The ratio of quasihexagonal domains to clusters increases with increasing temperature in our specimens.
3. The quasihexagonal domains have hexagonal order in some projections, and appear as equally spaced striations in others (Fig. 1, *C–F*; Fig. 3, *A* and *B*). Specimens temperature-jumped to $T > T_H$ after acidification at 2°C also contained extensive quasihexagonal domains (data not shown).
4. However, despite the similarity of the appearance of the quasihexagonal domains to the appearance expected for bulk H_{II} phase, the quasihexagonal domains do not represent an equilibrium H_{II} phase. The apparent unit cell spacing in the hexagonal cross-sections and the spacing of the striations are both significantly different from those expected for an H_{II} phase, at least at the lower temperatures (21–27°C).
5. More important, the DSC and time-resolved ^{31}P-NMR data show that no equilibrium H_{II} phase forms in acidified LUV dispersions below the T_H as measured for multilamellar dispersions. The DSC data (Fig. 4) show that at least most of the lipid was available for H_{II} formation at T_H when LUVs were acidified at the temperatures of our TRC-TEM study. The time-resolved ^{31}P-NMR data (Fig. 5) show that LUV dispersions are in the lamellar phase 1–2 min after acidification at the same temperatures. Therefore, the quasihexagonal domains imaged by TRC-TEM do not represent an equilibrium H_{II} phase.
6. Structures with the small interfacial radii found in the quasihexagonal domains (Fig. 1, *C–F*; Fig. 2; Fig. 3, *A* and *B*) would produce either isotropic or other nonlamellar powder patterns in ^{32}P-NMR spectra. Since these contributions are largely (isotropic) or completely (hexagonal) absent from the time-resolved ^{31}P-NMR spectra, the quasihexagonal domains imaged via TRC-TEM must have decayed to multilamellar structure within as little as 1 min after acidification. This process appears to be underway in micrographs like Fig. 3, *A* and *B*.
7. In specimens acidified below T_H and temperature-jumped to $T > T_H$ 10 ms before vitrification (Fig. 1 *F*), the quasihexagonal domains seem to have grown to absorb almost all the lipid in the aggregates, and become very similar to the expected appearance of H_{II} phase. It is difficult to resolve the fine structure of these thick aggregates, but much of this morphology may indeed represent H_{II} phase, which would be the equilibrium phase after the temperature jump. Combined with earlier TRC-TEM results showing that the L_α/H_{II} transition occurs in 10 ms in egg PE under similar conditions (Siegel et al., 1994), these results indicate that quasihexagonal domains can rapidly expand into H_{II} phase.

What can we learn about the mechanism of the L_α/H_{II} phase transition from these results? The outlines of the transition process must be as follows. Previous experience (e.g., Siegel et al., 1989b, 1994; Hui et al., 1983; Verkleij, 1984) shows that the dimensions of the first connections between apposed bilayers during L_α/H_{II} and L_α/Q_{II} transitions are small (~10 nm or less in diameter). These initial connections must then rapidly (tens of milliseconds) aggregate into clusters, and then rearrange into a structure with long-range order and hexagonal symmetry in some projections. When heated above T_H, this quasihexagonal structure must be able to rapidly (~10 ms or less) form H_{II} phase domains.

Which models of the transition mechanism are capable of rationalizing these observations? To discuss this question, we must briefly review current models for the types of structures that form between apposed bilayers. The motivation for most work in this area has been to determine the structure of the intermediates that form in the process of membrane fusion.

The "stalk" mechanism of membrane fusion

Theoretical work on the mechanism of membrane fusion indicates that fusion proceeds via formation of so-called "stalks" and "hemifusion" intermediates (Markin et al., 1984; Leikin et al., 1987; Kozlov et al., 1989; Siegel, 1993). This mechanism is compatible with a wide range of observations on membrane fusion between pure lipid bilayers (Chernomordik et al., 1985, 1987, 1995b), and there is increasing evidence that proteins make use of similar intermediates in biomembrane fusion (Chernomordik et al., 1993, 1995a, c, 1997; Vogel et al., 1993). Stalks and the structures that form from them are the lowest energy intermembrane structures that have been proposed (Siegel, 1993). Moreover, when LUVs interact under conditions where lamellar-to-inverted phase transitions occur, interve-

sicular lipid mixing and limited fusion are observed (e.g., Ellens et al., 1985, 1986, 1989; Siegel et al., 1989a, b). Therefore, the same structures may form initially during lamellar/inverted phase transitions, which are also intermembrane processes. The model for the relative energy of intermediate structures used previously (Siegel, 1993) has been very successful. Other workers have shown that it quantitatively predicts most features of a complex portion of the phase diagram of DOPE in water (Kozlov et al., 1994), by correctly predicting the relative energies of the different lipid phases. Therefore, we can have some confidence in the model's predictions concerning the relative energies of different fusion intermediate structures.

The current theories of stalk-mediated fusion share the same general outline (Fig. 6). The first intermediates to form between apposed membranes are stalks, which are semitoroidal connections between apposed bilayers formed only from lipids in the facing monolayers of the two bilayers (Fig. 6 *B*). Stalks can expand radially to form hemifusion intermediates (also called TMCs; Siegel, 1993), as shown in Fig. 6 *C*. This process is driven by the attendant decrease in curvature energy of the exterior, semitoroidal monolayer (Markin et al., 1984). Siegel (1993) showed that radial expansion is opposed by two factors. Radial expansion requires an increase in curvature energy of the distal (*trans*) monolayer associated with formation of the curved periphery of the diaphragm. It also increases the perimeter of the hydrophobic interstice (the speckled areas in Fig. 1 *C* are cross-sections of the interstice), which is energetically unstable. These factors must be included in calculation of the energies of these intermediates. In the TMCs, the aqueous compartments of the two original vesicles are separated by a single bilayer diaphragm (the center of the structure in Fig. 6 *C*). Rupture of this diaphragm forms a fusion pore, or ILA (Fig. 6 *D*). The diaphragm of the TMC is under tension due to curvature and chain-packing stresses (Siegel, 1993). Rupture of the bilayer diaphragm is the last, critical step in the overall fusion process.

Formation of stalks and TMCs requires the least energy when the spontaneous curvature of the system has values corresponding to proximity to lamellar/inverted phase transitions (Siegel, 1993). Therefore, it makes sense to study fusion intermediates near L_α/Q_{II} and L_α/H_{II} phase boundaries, because the intermediates should be most numerous. In addition, calculations show that the stress on the diaphragm of TMCs is lowest in vicinity of these phase transitions. As a result, TMCs may be somewhat more stable under these conditions than with lipid compositions more like those of biomembranes (Siegel, 1993).

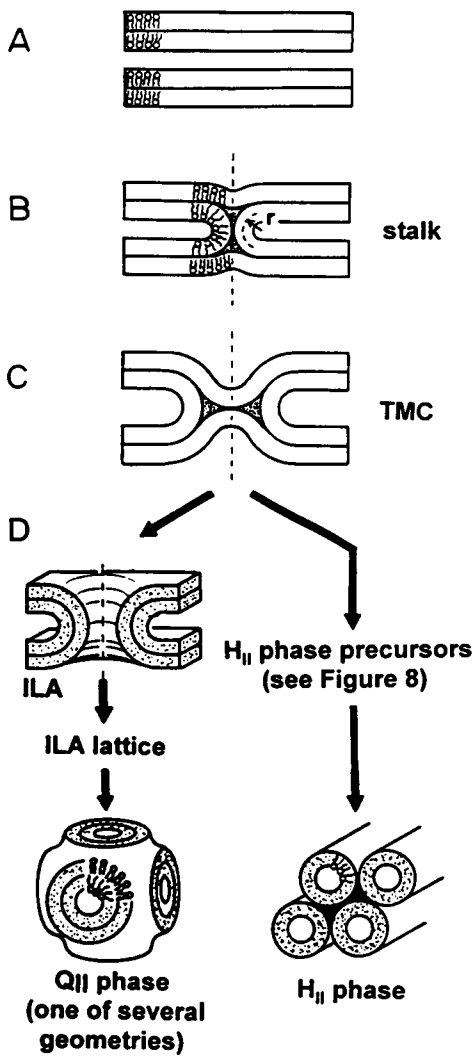

FIGURE 6 Modified stalk theory of membrane fusion and inverted phase formation. Monolayers of phospholipid are indicated as slabs. (*A*) Bilayers in the L_α phase. (*B*) Stalk. The structure is cylindrically symmetric around the dashed vertical axis, and is formed only from lipids in the apposed (*cis*) monolayers. (*C*) *trans* monolayer contact (TMC), or hemifusion intermediate. A TMC is formed by radial expansion of the semitoroidal exterior monolayer of the stalk. The distal (*trans*) monolayers above and below the stalk pinch inward to form a single bilayer diaphragm at the center of the TMC. (*D*) *Left:* Rupture of the diaphragm of the TMC produces a fusion pore, also termed an interlamellar attachment (ILA), shown here in cross-section. This corresponds to fusion (aqueous contents mixing) of two apposed LUVs. When ILAs accumulate in sufficient numbers, they form ILA lattices, which are intermediates in Q_{II} phase formation (see text). *Right:* Alternatively, for systems near the L_α/H_{II} phase boundary, TMCs can be sufficiently numerous to assemble into H_{II} precursors (see Fig. 8). In (*C*) and (*D*), the edges of lipid monolayers are stippled to emphasize the geometry of the different structures.

How might a stalk mechanism mediate lamellar/inverted phase transitions?

It is easy to see how Q_{II} phase can form from the L_α phase via this mechanism. Q_{II} phases can form once a large number of ILAs is present within a stack of bilayers. As the ILAs increase in number they will automatically form a lattice with the same connectivity as one of the infinite periodic surface-based Q_{II} phases (Siegel, 1986b). Formation of a Q_{II} phase of the Im3m symmetry from this geometry is facile, involving no further change of connectivity of the bilayers. It is notable that the other observed Q_{II} phase

geometries have the equivalent genus and are nearly isoenergetic, meaning that they should also easily interconvert via processes involving no changes in bilayer connectivity (Siegel, 1986b). The precursor lattice of ILAs has been observed via freeze-fracture electron microscopy in systems near the L_α/Q_{II} phase boundary (Siegel et al., 1989b). Note that ILAs are fusion pores. The correspondence between ILA formation and fusion in LUV systems has been established previously by many authors (Ellens et al., 1989; Siegel et al., 1989a, b, 1994; Frederik et al., 1989; Yeagle et al., 1991, 1994; van Gorkom et al., 1992; Lamparski et al., 1992; Ortiz et al., 1992; Epand et al., 1993).

It is more difficult to see how stalks and their progeny (Fig. 6) can rapidly form H_{II} phase domains. It is very unlikely that the L_α phase bilayers form ripples and merge with apposed bilayers simultaneously all along the crests of the ripples. Rippling the bilayers in this manner requires a very large input of activation energy. Moreover, the amount of activation energy necessary to merge two apposed bilayer-water interfaces grows with the amount of area over which the merging event must occur. The activation energy per unit area of apposed interface is substantial: strong short-range repulsive forces between interfaces must be overcome, favorable interactions between adjacent lipid molecules must be disrupted, and hydrophobic moieties must be transiently exposed to water. Therefore, the activation for such a concerted tube formation mechanism would be enormous, resulting in a rate too slow to explain observed transition times (as fast as 10 ms). It is much more likely that small connections between apposed bilayers are made first, which require much lower activation energies, and that these initial connections then somehow extend to form domains of H_{II} phase via a lipid diffusion-controlled process.

This concept is the basis for previously proposed L_α/H_{II} transition mechanisms, in which the first intermembrane structures were either stalklike objects (Hui et al., 1983; Caffrey, 1985; Siegel et al., 1994) or inverted micellar intermediates (Siegel, 1986a). The inverted micellar intermediate model was later discarded, since the activation energy for forming these structures was shown to be much larger than for stalk formation (Siegel, 1993). These models were all basically similar in the sense that individual interbilayer connections (or pairs of connections; Siegel, 1986a) were proposed to extend to form structures resembling the halves of two H_{II} tubes, apposed back-to-back. It was reasoned that such structures resembled the H_{II} phase closely enough so as to be nearly isoenergetic with it. Hence, when the transition temperature exceeded T_H, lipid would enter these structures rapidly by diffusion from contiguous bilayers, extending the structure to form H_{II}-like line defects, that would subsequently join side-to-side to form domains of H_{II} phase. However, in the light of subsequent data and theoretical work, it now appears that the isolated defect elongation espoused by all these models is unrealistic. Calculations of the energies of these line defects, using the methods of Siegel (1993), show that such structures would be unstable at temperatures near T_H, and would not form spontaneously until the temperature increased to $\sim 100°$ above T_H. Therefore, these structures cannot rationalize the quasihexagonal morphology that we observe at temperatures well below T_H, nor do they represent a reasonable pathway for the transition at $T = T_H$. The details of these calculations are presented elsewhere (Siegel, submitted for publication, 1997).

The reasons for the instability of the line defect intermediates lie in subtle differences between their structure and the structure of the H_{II} phase. Two possible cross-sections of the line defect invoked by the previous transition models are shown in Fig. 7 *A*. They differ in the curvature of the distal (*trans*) monolayers overlying the hydrophobic interstices in the structures (*stippled areas*). These line defects could be formed by elongation of a stalk along an axis perpendicular to its vertical axis, for instance. A cross-section of a unit cell of H_{II} phase is shown in Fig. 7 *B*. It is clear that the cross-sections of the line defects in Fig. 7 *B* resemble this unit cell. However, there are important differences between them. The top line defect structure in Fig. 7 *A* has hydrophobic interstices that are nearly three times as large as in the H_{II} phase. The reduction in curvature free energy obtained by forming the curved interfaces in the H_{II}

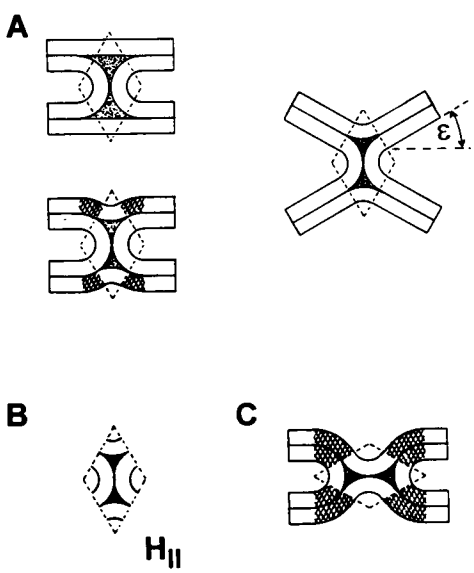

FIGURE 7 Comparison of the cross-sections of intermembrane intermediates with the cross-section of an H_{II} phase unit cell. Monolayers are depicted as slabs, and hydrophobic interstices as stippled areas. (*A*) Stalks. *Top*: Stalk with flat distal (*trans*) monolayers. *Bottom:* stalks with dimpled distal monolayers. The angle ϵ (*bottom right*) defines the extent to which the original lamellae are bulged toward each other at the periphery of the intermediate structure. ϵ is 0 for apposition of two flat bilayers. When $\epsilon = 0$, the stalk with dimpled *trans* monolayers (*bottom left*) has regions of monolayer with positive curvature, which is energetically unfavorable (cross-hatched region). (*B*) Unit cell of H_{II} phase. In (*A*) and (*C*), the diamond shapes drawn in dashed lines are the outline of regions most similar in cross-section to the H_{II} phase. (*C*) TMC. The cross-hatching indicates the regions of bent bilayer at the periphery of the structure, which have an unfavorable curvature energy.

phase is balanced by the energetically unfavorable creation of interstices (see Siegel, 1993, for references). The energy needed to create the interstices in the line defect structure is much larger than in the H_{II} phase. Moreover, the distal (*trans*) monolayers are flat in this cross-section, as opposed to curved, as in the H_{II} phase. The bottom line defect structure has smaller interstices, but now there are regions where the curvature of the *trans* monolayers is positive (i.e., energetically unfavorable). It can be shown that, because of these factors, neither of these line defects is capable of elongating into an H_{II}-like structure until the temperature is increased 100° or more above T_H (Siegel, manuscript in preparation). The only circumstances in which such defects can elongate spontaneously is when the local angle between the apposed interfaces (ϵ, Fig. 7 *A*) is nearly 30°. However, this is unlikely to be true for most of the closely apposed bilayers in a lamellar phase. It also requires that the bilayers be deformed into 30° bends along the entire periphery of the growing line defect. This requires the input of additional energy. (However, this might explain the very rare occurrence of line defectlike structures in circumstances where the bilayers seem to meet at 30° angles; Siegel et al., 1994.) Finally, elongation of individual line defect structures may not be able to form well-ordered domains of H_{II} phase as rapidly as is required to explain the fast transition times we and others have observed. In order to form bundles of H_{II} tubes, many line defects forming between a given pair of bilayers would have to align themselves with defects forming between adjacent pairs of bilayers on the same time scale as defect elongation. It is not clear how this can occur.

For these reasons, a stalk is very unlikely to grow into a H_{II}-like defect. In Fig. 7 *C*, we also show that an isolated TMC will not spontaneously elongate into a line defectlike structure. Although the cross-section of a TMC also contains the cross-section of a unit cell of H_{II} phase (*dashed lines*), the regions of bent bilayer at the periphery of the structure (*cross-hatched areas*) also have a large, unfavorable curvature energy, and keep the TMC from spontaneously elongating until the temperature is very far above T_H. These considerations show that isolated intermembrane connections like stalks and TMCs cannot mediate the L_α/H_{II} phase transition at T near T_H, and that line defects certainly cannot form at $T < T_H$, as would be required to explain the quasihexagonal morphology we observe in this work. How does the transition proceed, and what is the structural explanation of the quasihexagonal morphology?

Formation of H_{II} phase precursors by aggregation of TMCs

Using the model in Siegel (1993), it can be shown that TMCs should aggregate spontaneously to form an array that is more stable than the isolated TMCs. This process is depicted in Fig. 8. The dimensions of a TMC are determined by three parameters: the marginal radius r, dimple radius r_3, and marginal angle θ, as defined in Fig. 8 *A*. The highest-energy portions of TMCs are the bent bilayer segments at the periphery of the structure (i.e., the semitoroidal bilayer "skirt" of the TMC corresponding to a range of θ from ~30–90°). If TMCs within a stack of planar bilayers aggregate side-to-side as shown in Fig. 8 *B*, some of the bent bilayer segment area is eliminated. Small reductions in the angle θ at any value of r substantially reduce the TMC energy, while small changes in r and r_3 have little effect on the energy of the TMC (Siegel, 1993; submitted, 1997). Side-to-side aggregation of TMCs lets θ decrease and r increase in the region where the TMCs contact each other, reducing the total energy of the two aggregated TMCs below that of two isolated TMCs. The value of r changes in complementary fashion to θ around the periphery of the TMC, increasing where θ decreases. Therefore, distortion of a pair of TMCs as depicted in Fig. 8 *B* doesn't change the local spacing between the pairs of bilayers around the periphery of the TMCs. Each pair-wise interaction between TMCs should lower the total energy by several k_BT (where k_B is Boltzmann's constant). This is a fairly general property of the TMC geometry. If TMCs form at temperatures far below T_H, they should still show this tendency to aggregate, provided there are sufficient numbers of them and their lifetimes are long enough for them to encounter each other.

The aggregation process should continue in this pair-wise fashion until an extended aggregate forms with a body-centered cubic or primitive tetragonal symmetry. Within this aggregate, each TMC has eight nearest neighbors; four arranged in a square around the "top" of the central TMC, and four around the "bottom." A cross-section through this structure in the 110 plane is shown in Fig. 8 *C*. This TMC aggregate has two important properties. First, an individual TMC within the aggregate cannot revert to planar bilayer structure without simultaneously requiring its neighbors to revert to their original geometry (i.e., the local value of θ returns to 0), thereby raising the energy of all the neighboring TMCs. At temperatures below the L_α/H_{II} transition temperature, although the lipid in each individual TMC still has a slightly higher free energy than bilayer lipid, the activation energy for reversion is higher in a TMC aggregate than for isolated TMCs. In addition, reversion of a TMC within such an aggregate involves coordinated motions of lipids across a much larger structure than a single TMC, because of the involvement of neighboring TMCs. Hence the reversion rate of aggregated TMCs should be considerably slower than for isolated (unstable) TMCs, and the TMC array should be kinetically metastable.

The second important feature of the TMC aggregate is that it seems to offer a facile pathway for H_{II} phase formation at $T > T_H$. The geometry of the cross-section in Fig. 8 *C* is similar to a cross-section through an H_{II} phase domain (shown in Fig. 8 *D*). The cross-section contains distorted, closed cylinders of monolayer packed in a quasihexagonal fashion (i.e., each has six nearest neighbors, just as the H_{II} tubes do in Fig. 8 *D*). If the TMC aggregate is heated through T_H, lipid diffusion within the adjoining bilayers could cause this cross-section to extend out of the plane of

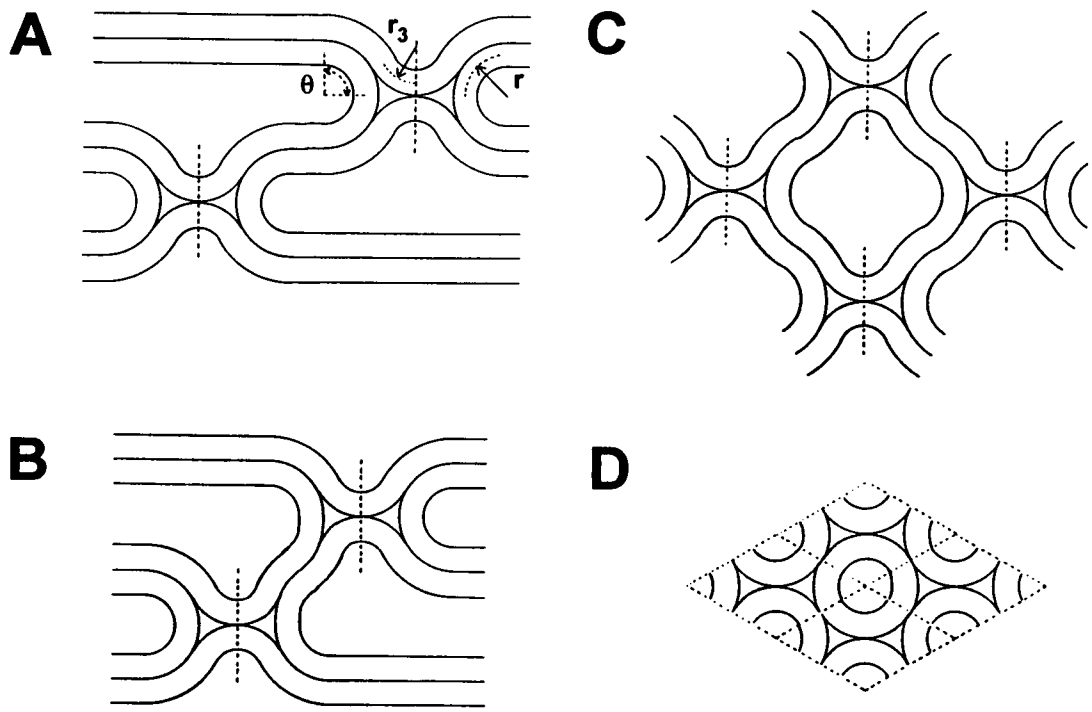

FIGURE 8 TMC aggregation. (*A*) Isolated TMCs within a set of apposed bilayers. r is the marginal radius, r_3 is the dimple radius of curvature, and θ is the marginal angle (90° when $\epsilon = 0$). (*B*) Side-to-side aggregation of two TMCs reduces θ and increases r around part of the periphery of each, where the two TMCs contact each other. The value of r changes in complementary fashion to θ around the periphery of each TMC, increasing where θ decreases. Therefore, the local spacing between the planar bilayers doesn't change. (*C*) The aggregation proceeds to form an aggregate with body-centered cubic or primitive tetragonal symmetry. Each TMC has eight nearest neighbors: four packed in a square around the "top" of the central TMC, and four around the "bottom." A cross-section in the 110 plane of this structure is shown. Note that the cross-section contains distorted, closed cylinders of monolayer packed in a quasihexagonal fashion (i.e., each has six nearest neighbors). At $T > T_H$, this structure could grow out of the plane of the paper to form a domain of H_{II} phase (with cross-section depicted in (*D*)).

the paper, collapsing into a more perfectly hexagonal geometry as it goes, thus growing directly into a domain of H_{II} phase. Therefore we propose that this is the mechanism of the L_α-to-H_{II} phase transition. That is, aggregates of TMCs form nuclei that can grow into H_{II} phase domains by lipid diffusion. However, it must be noted that the theoretical analysis in Siegel (1993) cannot make detailed predictions about the lowest energy geometry of the TMC array. In order to keep the mathematics tractable, the analysis assumes that all intermediate geometries are composed of segments of spheres, cylinders, cones, or circular toroids of revolution. In fact, much more complex TMC and TMC array geometries (e.g., catenoids, ellipsoids of revolution) might be involved. Therefore, it is possible that a different TMC aggregate geometry from the one in Fig. 8 *C* is involved. In particular, it may be that TMC arrays generate a cross-section that is much more similar to the H_{II} unit cell cross-section than depicted here.

In principle, stalks with dimpled *trans* monolayers (Fig. 7 *A*, *bottom left*) should also be capable of the same sort of aggregation process as depicted in Fig. 8, since side-to-side aggregation of such structures will also reduce the proportion of monolayer with unfavorable curvature energy. However, it is more probable that TMCs are the intermediates that pack in this manner. TMCs are lower in energy than stalks (Fig. 7 *A*, *bottom left*) for many values of r (Siegel, 1993; submitted, 1997). Presumably, stalks can also revert to a planar bilayer structure in a single step, whereas TMCs would have to radially contract back to stalks before reversion could occur (i.e, regression from Fig. 6 *B* to Fig. 6 *A* for stalks, versus regression from Fig. 6 *C* to 6 *A* for TMCs). Therefore, stalks are likely to be more labile than TMCs, and the steady-state concentration of stalks may be too low to form aggregates.

TMCs and TMC aggregates should be more common in LUV versus MLV systems

Previous time-resolved x-ray diffraction (Caffrey, 1985; Kriechbaum et al., 1989; Caffrey et al. 1990; Laggner and Kriechbaum, 1991; Laggner et al., 1991; Erramilli et al., 1995; Tate et al., 1992; Erbes et al., *Ber. Bunsenges. Phys. Chem.*, submitted) and electron microscopy (e.g., Verkleij et al., 1978, 1979; Rand et al., 1981; Hui and Stewart, 1981; Hui et al., 1983; Verkleij, 1984) studies of the L_α/H_{II} phase transition revealed no ordered arrays of transient intermediates. This contrasts with the predictions of the TMC-mediated transition mechanism discussed above. However, in the x-ray and electron microscopy studies the initial L_α

phase was present as well-ordered multilamellar preparations obtained by direct hydration of dry lipid (MLVs). Theory suggests that TMCs and TMC aggregates should be much more common when the transition starts in dispersions of LUVs. Rare TMC aggregates that form in MLVs could escape detection by x-ray diffraction and freeze-fracture electron microscopy. The x-ray diffraction patterns would be determined by the bulk of the (lamellar) phase lipid in the sample, while freeze-fracture EM examines only a very small fraction of the membrane in a dispersion (a single fracture plane).

The membranes at the periphery of the LUV-LUV contacts are nonplanar, while most of the bilayers in MLVs are nearly parallel. There are also many water passages around LUVs in an LUV aggregate, so that water transport into and within the planes of LUV-LUV contacts is much more rapid than between the bilayers of MLVs. Both of these factors should increase the initial formation rate of TMCs in LUVs relative to MLVs. TMCs are much lower in energy if the value of ϵ (Fig. 8 *A*) is > 0. [In PE, a TMC with $\epsilon = 30°$ has an energy that is only 40% of the energy of a TMC with $\epsilon = 0$; (Siegel, 1993).] The value of ϵ will be >0 around part of the circumference of TMCs forming near the periphery of LUV-LUV contacts. Thus, more TMCs should form per unit area around the periphery of LUV-LUV contacts than between the flat membranes within MLVs. Second, the "height" of a TMC (the distance between bilayers at the periphery of a TMC) is much greater than the equilibrium distance between PE bilayers near T_H. The "height" of a TMC is ~3–5 nm (Siegel, 1993), while the separation between PE interfaces in a multilamellar liposome is 1 nm or less (Rand et al., 1988). In order to form TMCs within MLVs, which are typically many μm in extent, a lot of water has to be transported within the plane of the bilayers, and across bilayers, to permit this local increase in bilayer separation. This is much easier to do in an aggregate of LUVs, since the contacts between LUVs are much smaller (~0.1 μm), and water has to be transported over smaller distances than in MLVs. [For a given pressure head, the flow rate of water between concentric lamellae is proportional to the cube of the interlamellar separation and the square of the radius (Byrd et al., 1960).] Note that the membrane curvature at the periphery of the LUV-LUV contact region is not due solely to the original shape of the vesicles: the strong adhesion energy of PE bilayers (McIntosh and Simon, 1996) distorts the vesicles so that as much of their surface area as possible becomes mutually apposed, strongly deforming the membranes at the periphery of the contacts (Fig. 1 *B*).

There is also experimental evidence that some types of long-range inverted phase order (like the TMC aggregates) can be achieved more easily in LUV dispersions. Ellens et al. (1989) found that the L_α/Q_{II} phase transition is more rapid in acidified LUV dispersions of DOPE-Me, as opposed to MLVs. Using freeze-fracture electron microscopy, they showed that acidified LUV dispersions formed large domains of Q_{II} phase within 10 min after acidification, whereas MLVs incubated under similar conditions showed only numerous ILAs and few if any Q_{II} inclusions. Later experiments (Siegel and Banschbach, 1990) showed that the L_α/Q_{II} phase transition in bulk multilamellar samples takes ~1 h. Time-resolved light scattering and fluorescence data (Ellens et al., 1989) also suggest that Q_{II} domain formation is more cooperative in LUVs than in MLVs, and occurs within only 1–2 min after acidification.

Key conclusions of the TMC-mediated transition theory

The key points of the theoretical analysis of the TMC-mediated mechanism are: 1) aggregates of TMCs should form spontaneously from isolated TMCs and be kinetically metastable; 2) the aggregates should form even at temperatures well below T_H if TMCs are sufficiently numerous and long-lived; 3) the aggregates provide a mechanism for nucleation and diffusion-driven growth of H_{II} phase domains. This is necessary to explain the rapid transitions that we and others observe. 4) TMCs and TMC aggregates should form more extensively between aggregated LUVs than in MLVs.

A TMC-mediated transition mechanism is the mechanism that is most compatible with our observations

In our view, the first step in the transition is formation of stalks (Fig. 6 *B*), which almost immediately expand to form TMCs (Fig. 6 *C*). The clusters of intermembrane connections visible in our TRC-TEM micrographs (Fig. 1, *C, E,* and *G*; Fig. 2; Fig. 3, *A* and *B*) may be mixtures of closely spaced TMCs and small aggregates of TMCs without long-range order (i.e., Fig. 8 *B*). The anticipated diameter of TMCs is ~9 nm or less (Siegel, 1993), and they would generate less contrast than ILAs. ILAs are larger (Siegel et al., 1989b, 1994), which increases the path length of electrons through the structure. This is compatible with the comparison of DiPoPE and DOPE-Me (ILA) morphology in Fig. 2. Moreover, we expect TMCs to form in large numbers at temperatures well below T_H. This is because the spontaneous curvature changes very slowly with temperature around T_H in PEs (Kozlov et al., 1994), and the energy of TMCs does not change rapidly with changes in spontaneous curvature amounting to changes of several tens of degrees (Siegel, 1993).

The next step in the transition should be formation of TMC aggregates with long-range order (Fig. 8 *C*). We propose that TMC aggregates may be the basis for the quasihexagonal domains that we observe at temperatures 20 or more degrees below T_H in DiPoPE (Fig. 1, *C–E, G*; Fig. 3, *A* and *B*). The TMC aggregate would appear to have hexagonal symmetry in some planes (the 110 plane depicted in Fig. 8 *C*). Moreover, TMCs should increase the local interlamellar spacing in a stack of bilayers to a value close to the tube diameter in the H_{II} phase (Siegel, 1993, and

manuscript in preparation). Therefore, well-ordered TMC aggregates and multilamellar stacks where there are many TMCs that have not yet aggregated into large arrays would both show intense striations with this spacing (~7 nm), as is observed. Since the energy of TMCs decreases slowly as the temperature increases in PE (Siegel, 1993), TMCs should become more numerous as the temperature increases, and thus form well-ordered aggregates more easily. This is compatible with the increase in proportion of quasihexagonal domain with increasing temperature. The TMC aggregates serve as H_{II} domain nuclei, and can elongate directly into H_{II} phase domains when $T > T_H$. This is compatible with the rapid formation of what appear to be domains of H_{II} phase in temperature-jumped DiPoPE specimens (Fig. 1 *F*), and the rapid L_α/H_{II} transition kinetics observed for egg PE in previous TRC-TEM work (Siegel et al., 1994).

However, the TMC aggregates are not stable: lipids in both isolated and aggregated TMCs are still at an energy above that of lipids in the L_α phase at $T < T_H$. Therefore, although aggregated TMCs will take longer to decay back to bilayer structure than isolated TMCs, the TMC aggregates must eventually decay to L_α phase. This is also compatible with our observations, since the time-resolved ^{31}P-NMR data show that most of the lipid is present as lamellar phase 1–2 min after acidification (Fig. 5) at temperatures where abundant quasihexagonal morphology is observed (Fig. 1 *E*; Fig. 3, *A* and *B*). The juxtaposition of quasihexagonal domains and multilamellar liposomes seconds after acidification (Fig. 1 *C*; Fig. 3, *A* and *B*) also suggests that the quasihexagonal domains rapidly decay into the equilibrium lamellar phase.

As discussed above, transition mechanisms based on line defect formation are incompatible with our data. First, we observed no individual line defects in our specimens, nor were they usually visible in DOPE-Me (Siegel et al., 1994). Second, line defects would not explain the H_{II}-like morphology that we observed at temperatures well below T_H. Our findings are quite consistent with the stalk/TMC theory of the fusion and phase transition mechanisms. However, the results are not sufficient to prove the mechanism because of three limitations inherent to the TRC-TEM technique. First, cryo-TEM is a low-contrast technique (Dubochet et al., 1988), and the exact structure of the first interbilayer intermediates cannot be demonstrated. Second, TEM only presents two-dimensional projections of three-dimensional objects. It is hard to establish the structure of complicated geometries like the postulated TMC arrays on this basis, particularly when the contrast problem limits the detail available about the TMC subunits when the overall structure is viewed at any but a few favored angles. Third, time-resolved TRC-TEM offers "snap-shots" of the transition process at different times after acidification of the dispersion, rather than a continuous record of the evolution of a given specimen. Therefore, it is difficult to establish the sequence of events in the transition scheme using only TRC-TEM data. In theory this can be done by varying the interval between acidification and vitrification. However, in practice the lipid aggregates grow too thick to be observed after only a few seconds, even at very low lipid concentration. Moreover, specimen-to-specimen variation in the details of the blotting procedure and variation in mixing times across the plane of the specimen can complicate interpretation (Siegel et al., 1989b, 1994).

Earlier observations on DOPE-Me LUVs (Siegel et al., 1994) are also compatible with a transition mechanism based on TMC aggregates. In the earlier study, the most striking intermediate structures were ILAs, whose structure is clearly discernible. However, in images of large DOPE-Me aggregates (e.g., Fig. 7 of Siegel et al., 1994), ILAs predominate in the periphery of the aggregates, but the interior seems to be composed of large numbers of somewhat smaller structures. These could be the same sort of intermediates as seen for DiPoPE (Fig. 2). In DOPE-Me, ILAs are required to form the Q_{II} phase. TMCs probably can rupture to form ILAs more frequently than in DiPoPE, which would account for the differences in the appearance of the two systems. The faster ILA evolution rate in DOPE-Me may be due to a difference in Gaussian curvature modulus or membrane rupture tension between the two lipid systems, as discussed below (see section entitled "Speculation: composition-dependent changes in rupture tension may affect the extent of ILA production").

Intermediate evolution scheme

Fig. 9 summarizes our inferences about the evolution of transition intermediates in DiPoPE. The upper portion of the figure summarizes interactions between bilayers in acidified dispersions of LUVs. LUVs aggregate and begin forming intermembrane intermediates (stalks, then TMCs). Isolated TMCs then form aggregates, which are lower in energy than isolated TMCs, and which are kinetically metastable. If the temperature is above T_H, these aggregates can grow rapidly into H_{II} phase domains by a lipid diffusion-limited process. However, TMCs and TMC aggregates must revert back to equilibrium lamellar phase structure (MLVs) if the temperature is below T_H, consistent with our time-resolved ^{31}P-NMR data (Fig. 5 *B*). Individual TMCs can form ILAs. This is a comparatively rare event in DiPoPE, and a more common one in DOPE-Me (Fig. 2), which is consistent with the spontaneous formation of Q_{II} phases in DOPE-Me and not in DiPoPE. In parallel to the TMC-mediated events, aggregated LUVs can form MLVs by an adhesion energy-driven process, which may be the process visualized in Fig. 3 *C*. Consistent with this, TRC-TEM data show that MLV formation is the major process underway at low temperature (5°C; Fig. 1 *B* and data not shown), where few intermembrane connections are observed.

The lower part of Fig. 9 summarizes the interactions anticipated during a transition in MLVs (bulk L_α phase). As discussed above, TMCs and TMC aggregates should be rarer in MLVs compared to aggregated LUVs. However,

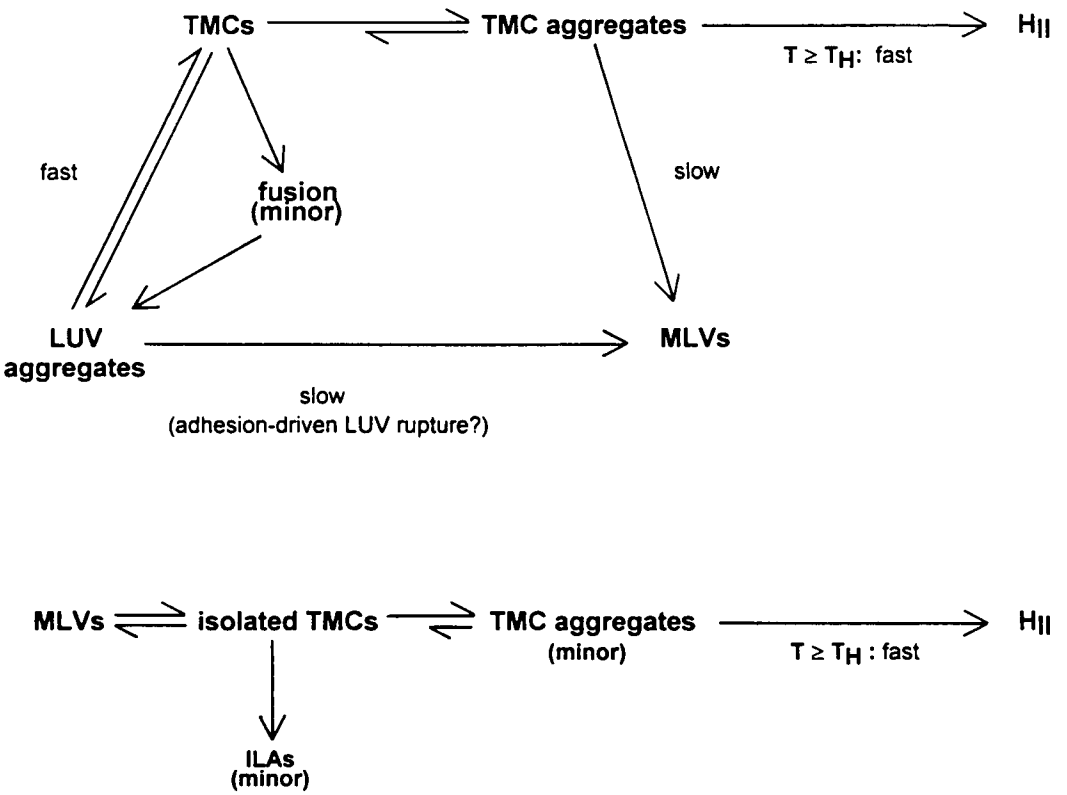

FIGURE 9 Intermediate evolution in DiPoPE. *Top:* The process that proceeds in acidified LUV dispersions. *Bottom:* Inferred process in MLV dispersions.

even if the number TMC aggregates is small, they can still generate a rapid L_α/H_{II} phase transition. It can be shown that, for an MLV sample at a temperature 1° above T_H, diffusion-limited growth of TMC aggregates 0.1 μm in diameter can generate a transition time of ~1 second when the TMC aggregates represent only 1% of the sample (Siegel, submitted for publication, 1997). As in LUV aggregates, a very small fraction of the TMCs may form ILAs in lipids like DiPoPE, and more in a lipid like DOPE-Me, which forms Q_{II} phases spontaneously at T near T_H.

Implications for the mechanism of membrane fusion

Our results provide strong support for the modified stalk theory of membrane fusion. The most surprising aspect of our observations is the existence of a long-lived, ordered array of transition intermediates (quasihexagonal domains). The modified stalk theory (Siegel 1993, and above) rationalizes this observation. Moreover, the TMC aggregate, which we propose is responsible for the quasihexagonal domains, provides a plausible mechanism for a fast L_α/H_{II} phase transition mechanism, while previously proposed transition mechanisms do not. While we cannot yet directly demonstrate the structure of the individual intermembrane connections, the sum of our observations is quite compatible with the modified stalk mechanism. The same intermediate structures (stalks and TMCs) that are involved in this transition mechanism are thought to mediate membrane fusion in uncharged or poorly charged lipid systems (Siegel, 1993). This is on account of the fact that stalks and TMCs appear to be the lowest energy continuous-monolayer structures that can form between apposed membranes, the starting point for both fusion and the L_α/H_{II} phase transition. Thus, our results also support a modified stalk mechanism of membrane fusion.

The TMC is a critical intermediate in both fusion and lamellar/inverted phase transitions. As shown in Fig. 9, the proportion of ILAs formed during bilayer-bilayer interactions is determined by the stability of the bilayer diaphragm of the TMC (Fig. 6 *C*) to rupture and form an ILA (fusion pore; Fig. 6 *D*, *left*). Presumably, this tendency influences the susceptibility of a lipid composition to fusion. It should also be noted that the transition mechanism in Fig. 6 is also consistent with the experimental linkage between Q_{II} phase formation and LUV fusion in phospholipid systems (e.g., Ellens et al., 1989; Siegel et al., 1989a, b; Nieva et al., 1995).

Comparison of the stalk/pore and modified stalk models of fusion intermediates

A TMC is also a transient intermediate in the stalk-pore mechanism of membrane fusion (e.g., Chernomordik et al.,

1995b). In the stalk-pore model, the initial stalk also radially expands into a TMC, but the TMC then continues to expand radially to form a single-bilayer diaphragm between the two apposed vesicles, termed a hemifusion intermediate. This extended bilayer diaphragm subsequently ruptures by formation of a semitoroidal aqueous pore within the bilayer. The modified stalk model (Siegel, 1993) predicts that TMCs will not radially expand in pure lipid systems, partly because this requires creation of longer, energetically unfavorable hydrophobic interstices. Thus one would expect TMCs to mediate fusion in pure lipid systems such as phospholipids. However, in systems where there is some apolar oil in the membranes, interstice energies diminish or disappear, just as H_{II} phase interstice energies are diminished in the presence of long-chain alkanes (e.g., Tate and Gruner, 1987). Therefore, TMCs should be free to radially expand into large, single-bilayer diaphragms in such cases. Accordingly, there is evidence for formation of large ($\sim$0.1–1 μm) hemifusion diaphragms during cell-planar membrane fusion (Melikyan et al., 1995), where the planar membranes probably retain traces of squalene. Biomembranes can contain significant levels of triglycerides, isoprenoid lipids, or other apolar components that could reduce or eliminate interstice energies, so that it's conceivable that large hemifusion diaphragms form during biomembrane fusion. However, hemifusion diaphragms are unlikely to form in pure phospholipids like DiPoPE, and we see no clear examples of them in the present study.

The rupture of a hemifusion diaphragm has been modeled as formation of a semitoroidal aqueous pore within the bilayer: the energy of this pore has been described in terms of the curvature energy of the pore edges (Kozlov et al., 1989; Nanavati et al., 1992). In the stalk-pore model, a surface tension in the two originally apposed bilayers is also required to stabilize pores above a certain critical diameter (Kozlov et al., 1989; Nanavati et al., 1992). If this description of the rupture event is correct, rupture requires a large activation energy. Even in the presence of surface tensions of 1 mN/m, large amounts of energy (100 k_BT or more) can be required to expand a pore to a size (>10 nm) from which it will spontaneously expand (Nanavati et al., 1992), irreversibly fusing the two original liposomes. However, it should also be noted that experimental values for the energy per unit length of pore edge in planar lipid bilayers (e.g., Chernomordik et al., 1985) and in pure phospholipid systems (Zhelev and Needham, 1993) are 10 or more times smaller than estimates made on the basis of curvature energy calculations. Therefore, pore formation may require less energy than expected because of the involvement of unknown factors.

In contrast, diaphragm rupture in the TMC is viewed as a highly localized event (Fig. 6, *C* and *D*): no lipid molecule's center of mass has to travel more than 1 or 2 nm to complete the rearrangement into a fusion pore. The diaphragm of a TMC is under stress, due to the curvature and interstice energies of the monolayers (Siegel, 1993). This stress is inherent in the geometry of the TMC: it is not an additional activation energy that must be assembled through thermal fluctuations after TMC formation. Siegel (1993) proposed that, if the stress is sufficiently large, the diaphragm will rupture, permitting rearrangement of the lipids into the monolayer lining of a fusion pore. The stress is a function of the spontaneous curvature of the lipid system. For example, using spontaneous curvature and elastic coefficient values for DOPE (Kozlov et al., 1994), it can be shown that the monolayers are stressed by $\sim$3 mN/m with respect to planar monolayers (Siegel, 1993; submitted, 1997). These estimates of the stress are likely to be overestimates, because the energy per unit area of the diaphragm lipid is different from the energy of the lipid in contiguous monolayers, and interdiffusion will reduce this gradient. However, it is clear that the stress is initially substantial. How can we tell if the estimated stress is sufficient to rupture the diaphragm of the TMC, as required for TMC-mediated fusion?

TMC diaphragm rupture and observed membrane rupture tensions

One approach is to postulate a specific geometry for the maximum-energy intermediate that forms during the process of rupture (like the pore of the stalk-pore model), and compare its energy with the integrated stress on a TMC diaphragm. However, rupture is an event that involves a handful of lipid molecules, in highly transient assemblies, and radii of curvature smaller than a molecular length. Our models for intermediate geometry and energy (e.g., Markin et al., 1984; Siegel, 1993) may be incomplete or invalid on those scales, as suggested by the disparity between estimated and measured pore edge energies. We therefore take a model-independent, observational approach: we compare the stress present in a TMC diaphragm with the measured stress required to achieve a similar rupture event. Evans and Needham (1986, 1987) measured the dilational work per unit area of membrane that has to be done to burst a unilamellar liposome. We suggest that the initial event in liposomal rupture under these conditions probably resembles the rupture event in TMC diaphragms. Presumably, in both cases the membrane is subjected to a two-dimensionally symmetric stress, which produces a local failure of cohesion in the membrane in a region only a couple of molecules wide. Evans and Needham found that stresses of several mN/m (3 mN/m for egg PC) had to be applied to bilayers in order to rupture them; close to the values anticipated in TMC diaphragms. Therefore, TMCs should be capable of spontaneously forming fusion pores, consistent with their postulated role in fusion (Siegel, 1993). Interestingly, the stress per unit area on the TMC diaphragm decreases as the system approaches T_H (Siegel, 1993; submitted, 1997), suggesting that TMCs show less and less tendency to form ILAs as the system approaches the L_α/H_{II} transition. This is consistent with the postulated role of TMCs (Fig. 7) in forming the H_{II} precursors observed in this work.

Note that we make no postulate as to the specific intermediate that forms in the course of TMC diaphragm rupture: it may well resemble the pore of the stalk-pore model of fusion. We only suggest that mechanically induced liposome rupture (Evans and Needham, 1986, 1987) is probably a very similar process on a microscopic scale, and that observed values of liposome rupture tension can be used to validate fusion mechanisms. It may also be possible to study composition effects on one aspect of fusion intermediate evolution using this technique.

Radial expansion of the TMC into a hemifusion diaphragm, as in the stalk-pore model (e.g., Kozlov et al., 1989; Nanavati et al., 1992), dilutes the stress on the TMC diaphragm by creating an extended diaphragm of planar membrane with no curvature or interstice stress. It may be that in systems that can form extended hemifusion diaphragms, fusion from a given stalk-initiated event is most likely just as the TMC forms, before it expands radially, and can only occur at a slower rate in the subsequently formed hemifusion diaphragm. Interestingly, the combined stresses on both monolayers of a TMC in PE are still substantial ($\sim$1 mN/m) in the absence of interstice energy. This means that diaphragm rupture is still possible in a TMC before it expands radially in hemifusing systems.

Speculation: composition-dependent changes in rupture tension may affect the extent of ILA production

Changes in bilayer composition affect the spontaneous curvature, and hence the relative energy, of TMCs and ILAs. We speculate that there may also be more subtle composition-dependent effects on rupture tension, as well, which could also affect the number of ILAs formed in a system, and thus change the rate of fusion in LUVs and the rate of Q_{II} phase formation. These effects could be demonstrated if there are changes in composition of a lipid mixture near the lamellar/inverted phase boundary that 1) have either no effect or very small effects on spontaneous curvature and the curvature elastic coefficient; 2) either increase the fusion rate of LUVs or increase the formation rate of ILAs and Q_{II} phase; and 3) lower the liposomal rupture tension.

We suggest that there are composition effects with these attributes. One mol % of a polyleucine peptide (Lys-Leu_{16}-Lys) lowers the rupture tension of phospholipid membranes by 50% (Evans and Needham, 1987). Similar mol fractions of the hydrophobic and amphipathic peptides alamethicin (Keller et al., 1996) and viral fusion peptides (Colotto et al., 1996; Colotto and Epand, 1997) can induce spontaneous formation of Q_{II} phase in PEs, which do not otherwise form Q_{II} phases without temperature-cycling. The peptides probably do not substantially affect the mean curvature energy of the host lipid, because they act at very low mol fractions ($<$1 mol %) and have either no effect or small effects on the lattice dimensions of the Q_{II} and H_{II} phases as a function of concentration. Therefore, alamethicin and the fusion peptides may not accelerate Q_{II} phase formation by changing the curvature energy of an intermediate or the equilibrium phase. These low levels of peptides are enough for the system to have, on average, one peptide molecule adsorbed to an area of bilayer equivalent to a TMC diaphragm. Perhaps the peptides act by lowering the rupture tension of the TMC diaphragm, just as the polyleucine peptide does in PC membranes (Evans and Needham, 1987). This probably occurs through a peptide effect on the cohesion of the lipid membrane [e.g., through a local change of bilayer thickness around an adsorbed peptide; He et al. (1996)]. Prenner et al. (1997) found that gramicidin S peptides also induce ILA and Q_{II} phase formation in some phospholipids. Gramicidin S peptides may act via a related mechanism. If peptides do act in this manner, it suggests that amphipathic or hydrophobic moieties on the lumenal domains of fusion proteins could help catalyze fusion by destabilizing the diaphragm of an adjacent TMC. It is also possible that the very different rates of ILA and Q_{II} phase formation in DOPE versus both DOPE/DOPC and DOPE-Me (Gruner et al., 1988; Shyamsunder et al., 1988; Ellens et al., 1989; Siegel and Banschbach, 1990) might be due in part to an effect of PC or headgroup methylation on membrane rupture tension. For instance, there is an intriguing hint that increases in the mol fraction of PC decrease the rupture tension of PE/PC mixtures (Evans and Needham, 1986, 1987). However, these speculations are based on a very limited number of rupture tension measurements. Moreover, extensive experiments would be required to determine the effects of the peptides on the equilibrium (thermodynamic) stability of the Q_{II} phase, which might also generate the experimental observations. For instance, the peptides might induce Q_{II} phase via a length mismatch effect (Killian et al., 1996), an effect on the Gaussian curvature modulus, or an effect on the chain-packing energy (Anderson et al., 1988) via local effects on bilayer thickness (e.g., He et al., 1996). This speculation will be discussed in more detail elsewhere (Siegel, submitted for publication, 1997).

CONCLUSIONS

Our data indicate that the same intermediates that form according to the modified stalk theory of membrane fusion also form during the L_α/H_{II} and L_α/Q_{II} phase transitions in PE and PE analogs. This transition mechanism is also consistent with data available for other PE and *N*-monomethylated PE systems (Siegel et al., 1989b, 1994). It makes sense to study the fusion intermediates in this context because of the large numbers and greater stability of the intermediates in the vicinity of lamellar/inverted phase transitions.

We cannot directly demonstrate the structure of the first intermediates in these processes (presumably, stalks and TMCs) with TRC-TEM.

However, the most striking feature of our TRC-TEM results is the presence of arrays of intermediate structures

(quasihexagonal domains) with lifetimes of seconds when the L_α/H_{II} transition starts in dispersions of LUVs. According to the modified stalk theory, the quasihexagonal domains are crystallites of fusion intermediates (TMCs; Fig. 8 *C*). Using stopped-flow mixing of highly concentrated LUVs, it may be possible to form transient quasihexagonal domains large enough for study via synchrotron-source time-resolved x-ray diffraction. If successful, this would directly demonstrate the structure of the fusion intermediates.

If the modified stalk theory is correct, the TMC is the critical intermediate that determines the extent of membrane fusion, and the rate of Q_{II} phase evolution, for PE and PE analog systems in the vicinity of T_H. We speculate that the inherent material strength of the bilayer diaphragm of the TMC is one factor that determines the rate and extent of these processes, and that measurements of the mechanical rupture tension of liposomal membranes can be used to measure composition-dependent changes in this strength. It is possible that hydrophobic peptides and viral fusion peptides promote fusion in model systems by destabilizing TMC diaphragms.

D.P.S. is grateful for the technical assistance of N. L. Reeder, and the technical advice of J. L. Burns, Z. Lin, and Y. Talmon. R.M.E. is grateful for the assistance of Raquel F. Epand and to Don Hughes for assistance in acquiring the NMR spectra.

This work was supported in part by the Medical Research Council of Canada Grant MT-7654.

REFERENCES

Anderson, D. M., S. M. Gruner, and S. Leibler. 1988. Geometrical aspects of the frustration in the cubic phases of lyotropic liquid crystals. *Proc. Natl. Acad. Sci. USA.* 85:5364–5368.

Bellare, J. R., H. T. Davis, L. E. Scriven, and Y. Talmon. 1988. Controlled environment vitrification system: an improved sample preparation technique. *J. Electron Microsc. Tech.* 10:87–111.

Booy, F. P., and J. B. Pawley. 1993. Cryo-crinkling: what happens to carbon films on copper grids at low temperature. *Ultramicroscopy.* 48:273–280.

Byrd, R. B., W. E. Stewart, and E. N. Lightfoot. 1960. Transport Phenomena. John Wiley & Sons, New York. 117–118.

Caffrey, M. 1985. Kinetics and mechanism of the gel/lamellar liquid crystal and lamellar/inverted hexagonal phase transition in phosphatidylethanolamine: a real-time x-ray diffraction study using synchrotron radiation. *Biochemistry.* 24:4826–4844.

Caffrey, M., R. L. Magin, B. Hummel, and J. Zhang. 1990. Kinetics of the lamellar and hexagonal phase transitions in phosphatidylethanolamine. Time-resolved x-ray diffraction study using a microwave-induced temperature jump. *Biophys. J.* 58:21–29.

Chernomordik, L. V., M. M. Kozlov, G. B. Melikyan, I. G. Abidor, V. S. Markin, and Yu. A. Chizmadzhev. 1985. The shape of lipid molecules and monolayer membrane fusion. *Biochim. Biophys. Acta.* 812: 643–655.

Chernomordik, L. V., G. B. Melikyan, and Yu. A. Chizmadzhev. 1987. Biomembrane fusion: a new concept derived from model studies using two interacting planar lipid bilayers. *Biochim. Biophys. Acta.* 906: 309–352.

Chernomordik, L. V., S. S. Vogel, A. Sokoloff, H. O. Onaran, E. A. Leikina, and J. Zimmerberg. 1993. Lysolipids reversibly inhibit Ca^{2+}-, GTP-, and pH-dependent fusion of biological membranes. *FEBS Lett.* 318:71–76.

Chernomordik, L. V., and J. Zimmerberg. 1995a. Bending membranes to the task: structural intermediates in bilayer fusion. *Curr. Opin. Struct. Biol.* 5:541–547.

Chernomordik, L., A. Chanturiya, J. Green, and J. Zimmerberg. 1995b. The hemifusion intermediate and its conversion to complete fusion: regulation by membrane composition. *Biophys. J.* 69:922–929.

Chernomordik, L., M. M. Kozlov, and J. Zimmerberg. 1995c. Lipids in biological membrane fusion. *J. Membr. Biol.* 146:1–14.

Chernomordik, L. V., E. Leikina, V. Frolov, P. Bronk, and J. Zimmerberg. 1997. An early stage of membrane fusion mediated by the low pH conformation of influenza hemagglutinin depends upon membrane lipids. *J. Cell Biol.* 136:81–93.

Colotto, A., and R. M. Epand. 1997. Structural study of the relationship between the rate of membrane fusion and the ability of the fusion peptide of influenza virus to perturb bilayers. *Biochemistry.* 36:7644–7651.

Colotto, A., I. Martin, J. M. Ruysschaert, A. Sen, S. W. Hui, and R. M. Epand. 1996. Structural study of the interaction between the SIV fusion peptide and model membranes. *Biochemistry.* 35:980–989.

Cullis, P. R., B. de Kruijff, M. J. Hope, A. J. Verkleij, R. Nayar, S. B. Farren, C. Tilcock, T. D. Madden, and M. B. Bally. 1983. Structural properties of lipids and their functional roles in biological membranes. *In* Membrane Fluidity in Biology, Vol. 1. R. C. Aloia, editor. Academic Press, New York. 39–81.

Dubochet, J., M. Adrian, J.-J. Chang, J.-C. Homo, J. Lepault, A. McDowall, and P. Schultz. 1988. Cryo-electron microscopy of vitrified specimens. *Q. Rev. Biophys.* 21:129–228.

Ellens, H., J. Bentz, and F. C. Szoka. 1985. Destabilization of phosphatidylethanolamine liposomes at the hexagonal phase transition temperature. *Biochemistry.* 25:285–294.

Ellens, H., J. Bentz, and F. C. Szoka. 1986. Fusion of phosphatidylethanolamine liposomes and the mechanism of the L_α-H_{II} phase transition. *Biochemistry.* 25:4141–4147.

Ellens, H., D. P. Siegel, D. Alford, P. L. Yeagle, L. Boni, L. J. Lis, P. J. Quinn, and J. Bentz. 1989. Membrane fusion and inverted phases. *Biochemistry.* 28:3692–3703.

Epand, R. M. 1990. Hydrogen bonding and the thermotropic transitions of phosphatidylethanolamines. *Chem. Phys. Lipids.* 52:227–230.

Epand, R. M., R. F. Epand, C. D. Richardson, and P. L. Yeagle. 1993. Structural requirements for the inhibition of membrane fusion by carbobenzoxy-D-Phe-Phe-Gly. *Biochim. Biophys. Acta.* 1152:128–134.

Erramilli, S., F. Osterberg, S. M. Gruner, M. W. Tate, and M. Kriechbaum. 1995. Time-resolved x-ray studies on pressure-jump induced topological transitions in biological membranes. *SPIE* 2521:188–196.

Evans, E., and D. Needham. 1986. Giant vesicle bilayers composed of lipids, cholesterol and peptides. *Faraday Discuss. Chem. Soc.* 81: 267–280.

Evans, E., and D. Needham. 1987. Physical properties of surfactant bilayer membranes: thermal transitions, elasticity, rigidity, cohesion, and colloidal interactions. *J. Phys. Chem.* 91:4219–4228.

Frederik, P. M., K. N. J. Burger, M. C. A. Stuart, and A. J. Verkleij. 1991. Lipid polymorphism as observed by cryo-electron microscopy. *Biochim. Biophys. Acta.* 1062:133–141.

Frederik, P. M., M. C. A. Stuart, and A. J. Verkleij. 1989. Intermediary structures during membrane fusion as observed by cryo-electron microscopy. *Biochim. Biophys. Acta.* 979:275–278.

Gagné, J., L. Stamatatos, T. Diacovo, S. K. Hui, P. L. Yeagle, and J. R. Silvius. 1985. Physical properties and surface interactions of bilayer membranes containing N-methylated phosphatidylethanolamines. *Biochemistry.* 24:4400–4408.

Gruner, S. M., M. W. Tate, G. L. Kirk, P. T. C. So, D. C. Turner, C. P. S. Tilcock, and P. R. Cullis. 1988. X-ray diffraction study of the polymorphic behavior of N-methylated dioleoylphosphatidylethanolamine. *Biochemistry.* 27:2853–2866.

He, K., S. J. Ludtke, W. T. Heller, and H. W. Huang. 1996. Mechanism of alamethicin insertion into lipid bilayers. *Biophys. J.* 71:2669–2679.

Hui, S. W., and T. P. Stewart. 1981. "Lipidic particles" are intermembrane attachment sites. *Nature (Lond.).* 287:166–167.

Hui, S. W., T. P. Stewart, and L. T. Boni. 1983. The nature of lipidic particles and their roles in polymorphic transitions. *Chem. Phys. Lipids.* 33:113–126.

Keller, S. L., S. M. Gruner, and K. Gawrisch. 1996. Small concentrations of alamethicin induce a cubic phase in bulk phosphatidylethanolamine mixtures. *Biochim. Biophys. Acta.* 1278:241–246.

Killian, J. A., I. Salemink, M. R. R. de Planque, G. Lindblom, R. E. Koeppe III, and D. V. Greathouse. 1996. Induction of nonbilayer structures in diacylphosphatidylcholine model membranes by transmembrane α-helical peptides: importance of hydrophobic mismatch and proposed role of tryptophans. *Biochemistry.* 35:1037–1045.

Koynova, R., and M. Caffrey. 1994. Phases and phase transitions of the hydrated phosphatidylethanolamines. *Chem. Phys. Lipids.* 69:1–34.

Kozlov, M. M., S. L. Leikin, L. V. Chernomordik, V. S. Markin, and Y. A. Chizmadzhev. 1989. Stalk mechanism of vesicle fusion. Intermixing of aqueous contents. *Eur. Biophys. J.* 17:121–129.

Kozlov, M. M., S. Leikin, and R. P. Rand. 1994. Bending, hydration, and interstitial energies quantitatively account for the hexagonal-lamellar-hexagonal reentrant phase transition in dioleoylphosphatidylethanolamine. *Biophys. J.* 67:1603–1611.

Kriechbaum, M., G. Rapp, J. Hendrix, and P. Laggner. 1989. Millisecond time-resolved x-ray diffraction on liquid-crystalline phase transitions using infrared laser T-jump technique and synchrotron radiation. *Rev. Sci. Instrum.* 60:2541–2544.

Laggner, P., and M. Kreichbaum. 1991. Phospholipid phase transitions: kinetics and structural mechanisms. *Chem. Phys. Lipids.* 57:121–145.

Laggner, P., M. Krecihbaum, and G. Rapp. 1991. Structural intermediates in phospholipid phase transitions. *J. Appl. Crystallogr.* 24:836–842.

Lamparski, H., U. Liman, J. A. Barry, D. A. Frankel, V. Ramaswami, M. F. Brown, and D. F. O'Brien. 1992. Photoinduced destabilization of liposomes. *Biochemistry.* 31:685–694.

Leikin, S. L., M. M. Kozlov, L. V. Chernomordik, V. S. Markin, and Y. A. Chizmadzhev. 1987. Membrane fusion: overcoming of the hydration barrier and local restructuring. *J. Theor. Biol.* 129:411–425.

Markin, V. S., M. M. Kozlov, and V. L. Borovjagin. 1984. On the theory of membrane fusion. The stalk mechanism. *Gen. Physiol. Biophys.* 5:361–377.

McIntosh, T. J., and S. A. Simon. 1996. Adhesion between phosphatidylethanolamine bilayers. *Langmuir.* 12:1622–1630.

Melikyan, G. B., J. M. White, and F. S. Cohen. 1995. GPI-anchored influenza hemagglutinin induces hemifusion to both red blood cell and planar bilayer membranes. *J. Cell Biol.* 131:679–691.

Nanavati, C., V. S. Markin, A. F. Oberhauser, and J. M. Fernandez. 1992. The exocytotic fusion pore modeled as a lipidic pore. *Biophys. J.* 63:1118–1132.

Nieva, J. L., A. Alonso, G. Basáñez, F. M. Goñi, A. Gulik, R. Vargas, and V. Luzzati. 1995. Topological properties of two cubic phases of a phospholipid:cholesterol:diacylglycerol aqueous system and their possible implications in the phospholipase C-induced liposome fusion. *FEBS Lett.* 368:143–147.

Ortiz, A., F. J. Aranda, J. Villalain, C. San Martin, V. Micol, and J. C. Gomez-Fernandez. 1992. 1,2-Dioleoylglycerol promotes calcium-induced fusion in phospholipid vesicles. *Chem. Phys. Lipids.* 62: 215–224.

Prenner, E. J., R. N-A. H. Lewis, K. C. Neuman, S. M. Gruner, L. H. Kondejewski, R. S. Hodges, and R. N. McElhaney. 1997. Nonlamellar phases induced by the interaction of Gramicidin S with lipid bilayers. A possible relationship to membrane-disrupting activity. *Biochemistry.* 36: 7906–7916.

Rand, R. P., N. Fuller, V. A. Parsegian, and D. C. Rau. 1988. Variation in hydration forces between neutral phospholipid bilayers: evidence for hydration attraction. *Biochemistry.* 27:7711–7722.

Rand, R. P., T. S. Reese, and R. G. Miller. 1981. Phospholipid bilayer deformations associated with interbilayer contact and fusion. *Nature (Lond.).* 293:237–238.

Shyamsunder, E., S. M. Gruner, M. W. Tate, D. C. Turner, P. T. C. So, and C. P. S. Tilcock. 1988. Observation of inverted cubic phase in hydrated dioleoylphosphatidylethanolamine membranes. *Biochemistry.* 27: 2332–2336.

Siegel, D. P. 1986a. Inverted micellar intermediates and the transitions between lamellar, cubic, and inverted hexagonal lipid phases. I. Mechanism of the L_α[dharrow]H_{II} phase transitions. *Biophys. J.* 49: 1155–1170.

Siegel, D. P. 1986b. Inverted micellar intermediates and the transitions between lamellar, cubic, and inverted hexagonal amphiphile phases. III. Isotropic and inverted cubic state formation via intermediates in transitions between L_α and H_{II} phases. *Chem. Phys. Lipids.* 42:279–301.

Siegel, D. P. 1993. The energetics of intermediates in membrane fusion: comparison of stalk and inverted micellar intermediate mechanisms. *Biophys. J.* 65:2124–2140.

Siegel, D. P., J. L. Banschbach, D. Alford, H. Ellens, L. J. Lis, P. J. Quinn, P. L. Yeagle, and J. Bentz. 1989a. Physiological levels of diacylglycerols in phospholipid membranes induce membrane fusion and stabilize inverted phases. *Biochemistry.* 28:3703–3709.

Siegel, D. P., and J. L. Banschbach. 1990. Lamellar/inverted cubic (L_α/Q_{II}) phase transition in N-methylated dioleoylphosphatidylethanolamine. *Biochemistry.* 29:5975–5981.

Siegel, D. P., J. L. Burns, M. H. Chestnut, and Y. Talmon. 1989b. Intermediates in membrane fusion and bilayer/nonbilayer phase transitions imaged by time-resolved cryotransmission electron microscopy. *Biophys. J.* 56:161–169.

Siegel, D. P., W. J. Green, and Y. Talmon. 1994. The mechanism of lamellar-to-inverted hexagonal phase transitions: a study using temperature-jump cryoelectron microscopy. *Biophys. J.* 66:402–414.

Talmon, Y., J. L. Burns, M. H. Chestnut, and D. P. Siegel. 1990. Time-resolved cryotransmission electron microscopy. *J. Electron Microsc. Technol.* 14:6–12.

Tate, M. W., and S. M. Gruner. 1987. Lipid polymorphism of mixtures of dioleoylphosphatidylethanolamine and saturated and unsaturated phosphatidylcholines of various chain lengths. *Biochemistry.* 26:231–236.

Tate, M. W., and S. M. Gruner. 1989. Temperature dependence of the structural dimensions of the inverted hexagonal (H_{II}) phase of phosphatidylethanolamine-containing membranes. *Biochemistry.* 28:4245–4253.

Tate, M. W., E. Shyamsunder, S. M. Gruner, and K. L. D'Amico. 1992. Kinetics of the lamellar-inverse hexagonal phase transition determined by time-resolved x-ray diffraction. *Biochemistry.* 31:1081–1092.

van Gorkom, L. C. M., S.-Q. Nie, and R. M. Epand. 1992. Hydrophobic lipid additives affect membrane stability and phase behavior of N-monomethyldioleoylphosphatidyl-ethanolamine. *Biochemistry.* 31: 671–677.

Van Venetië, R., and A. J. Verkleij. 1981. Analysis of the hexagonal II phase and its relations to lipid particles and the lamellar phase. A freeze-fracture study. *Biochim. Biophys. Acta.* 645:262–269.

Verkleij, A. J. 1984. Lipidic intramembranous particles. *Biochim. Biophys. Acta.* 779:43–63.

Verkleij, A. J., C. Mombers, W. J. Gerritsen, L. Leunissen-Bijvelt, and P. R. Cullis. 1978. Fusion of phospholipid vesicles in association with the appearance of lipidic particles as visualized by freeze-fracturing. *Biochim. Biophys. Acta.* 555:358–361.

Verkleij, A. J., C. Mombers, J. Lenissen-Bijvelt, and P. H. J. Th. Ververgaert. 1979. Lipidic intramembranous particles. *Nature (Lond.).* 279: 162–163.

Verkleij, A. J., C. J. A. van Echteld, W. J. Gerritsen, P. R. Cullis, and B. De Kruijff. 1980. The lipidic particle as an intermediate structure in membrane fusion processes and bilayer to hexagonal H_{II} phase transitions. *Biochim. Biophys. Acta.* 600:620–624.

Vogel, S. S., E. A. Leikina, and L. V. Chernomordik. 1993. Lysophosphatidylcholine reversibly arrests exocytosis and viral fusion at a stage between triggering and membrane merger. *J. Biol. Chem.* 268: 25764–25768.

Walter, A., and J. Gutknecht. 1984. Monocarboxylic acid permeation through lipid bilayer membranes. *J. Membr. Biol.* 77:255–264.

Yeagle, P. L., R. M. Epand, C. D. Richardson, and T. D. Flanagan. 1991. Effects of the "fusion peptide" from measles virus on the structure of N-methyl dioleoylphosphatidylethanolamine membranes and their fusion with Sendai virus. *Biochim. Biophys. Acta.* 1065:49–53.

Yeagle, P. L., F. T. Smith, J. E. Young, and T. D. Flanagan. 1994. Inhibition of membrane fusion by lysophosphatidylcholine, *Biochemistry.* 33:1820–1827.

Zhelev, D., and D. Needham. 1993. Tension-stabilized pores in giant vesicles: determination of pore size and pore line tension. *Biochim. Biophys. Acta.* 1147:89–104.